CHAOTIC STRUCTURES IN CONDUCTIVITY MECHANISMS

by

H. Ahmet Yıldırım

B.S., Physics, Boğaziçi University, 1994

M.S., Physics, Sakarya University, 1998

Submitted to the Institute for Graduate Studies in
Science and Engineering in partial fulfillment of
the requirements for the degree of
Doctor of Philosophy

Graduate Program in Physics

Boğaziçi University

2005

ACKNOWLEDGEMENTS

First and foremost, I would like to thank my thesis co-adviser, Prof. Dr. Avadis Hacınlıyan who has given the encouragement and motivation that I needed throughout my academic life. I owe special thanks to my thesis adviser, Prof. Dr. Yani Skarlatos for his critical advice and support during the progress of my work. I am also grateful to all my committee members who have contributed advice. In addition, I would like to thank Gökhan Şahin for his friendship and support, especially with the computer work.

I would like to express my deep gratitude to my parents, Yusuf Kenan Yıldırım and Pakize Yıldırım for their emotional support. Finally, I would like thank to my wife, Sabriye Yıldırım and my children, Halit and Zeynep for their patience and support throughout my graduate student life.

ABSTRACT

CHAOTIC STRUCTURES IN CONDUCTIVITY MECHANISMS

Chaotic behavior in the transient current through thin Aluminum-PMMA-Aluminum films has been analyzed for times ranging up to 30000s, in the temperature range 293-363 K for applied voltages in the range 10-80V. The general shape of the data suggests a slow decay to a steady state value superimposed with broadband oscillations. The aperiodic and broadband behavior of the transient current reminds one of an underlying chaotic structure. Indeed time series analysis reveals a positive Liapunov exponent consistently and reproducibly throughout this range which gives strong evidence for chaoticity. Power law relaxation as reflected by the autocorrelation function and the positive Liapunov exponent show parallel behaviors as a function of applied electric field and temperature.

The stretched exponential behavior of the data suggests that the process can be seen as random walk between random sites. The qualitative behavior of the data can be understood in terms of a quenched disorder picture as first suggested by Erzan et.al.

ÖZET

AKIM GEÇİŞ MEKANİZMALARINDA KAOTİK YAPILAR

Alüminyum-PMMA-Alüminyum ince filmlerindeki akımın kaotik davranışı 30000 saniyeye kadar süreler için, 293K ile 363K sıcaklık aralığında ve 10V ile 80V arasındaki gerilim değerleri için incelenmiştir. Akımın aperiodik ve geniş bantlı yapısı koatik bir yapıyı çağrıştırmaktadır. Akımın zaman serisi analizinde bu aralıklar için tutarlı ve tekrarlanabilir pozitif Liapunov üsteli hesaplanmıştır. Pozitif Lyapunov üstelinin uygulanan elektrik alana ve sıcaklığa bağlı degişimi otokoralasyon fonksiyonu ile betimlenen üstel gevşeme yasası ile paralellik göstermektedir.

Verilerin gerilmiş üstel davranış süreci rastgele siteler arasında gerçekleşen bir rastgele yürüyüş olarak ifade edilebileceğini göstermektedir. Verilerin nitel davranışı ise Erzan ve arkadaşları tarafından ilk kez önerildiği gibi bastırılmış düzensizlik yardımı ile anlaşılabilir.

TABLE OF CONTENTS

LIST OF FIGURES

LIST OF TABLES

LIST OF SYMBOLS/ABBREVIATIONS

B	Diffusive coupling
D_f	Box-counting dimension
d_E	Embedding dimension
E	External field
E_{th}	Threshold value for the external field
e	Electronic charge
e_i	Eigenvector of the Jacobian matrix
F_d	Damping force
J	Polarization current
m	Embedding dimension of the reconstructed phase space
m_e	Electron mass
n	Number of the time steps
P	Polarization
q	Wave number
$R_d(k)$	Distance in d dimensions
s_n	Measurement taken at time step
T	Temperature
T_t	Transit time of the carrier front
t	Time
U	Energy density
V	Potential Difference
v_F	The Fermi velocity
$\vec{s}(k)$	Embedding vector
$\vec{y}(k)$	time delay vector
β_i	Stretching factor in d dimensions
β_{pf}	Pool-Frankel parameter
β_{sch}	Schottky parameter
ϵ	Dielectric constant

λ	electron phonon coupling
Λ_i	Eigenvalue of the Jacobian matrix
ρ_0	One dimensional electron density
ρ_m	The effective mass density of the CDW
$\rho(\cdot)$	Charge density wave function
τ	Delay time
ϕ_i	Quenched random variable

CDW	Charge Density Wave
PMMA	Polymethylmethacrylate

1. INTRODUCTION

In general chaos is defined as a state of disorder and irregularity. The word itself originates from Greek Mythology as, the most ancient of gods, the personification of the infinity of space preceding creation of the universe or the infinite crude and shapeless space that existed before the architect of the world introduced order and harmony [1]. In everyday life the word chaos is used to describe a similar concept. On the other hand chaos has a very different and specialized meaning in science. A very straightforward definition of chaos is sensitive dependence on initial conditions [2]. Another well known phrase to describe chaos is the butterfly effect "The flapping of a single butterfly's wing today produces a tiny change in the state of the atmosphere. As a result over a period of time, what the atmosphere actually does is widely different from what it would have done. So, in a month's time, a tornado that would have devastated the Indonesian coast doesn't happen, or maybe one that wasn't going to happen, does" [3]. But the phrase " chaotic motion " does not imply that the behavior of the system is frenzied or wild in appearance. In fact a system which appears to be smooth or ordered can actually be a chaotic one. Rather, chaos refers to the issue of whether or not it is possible to make accurate long-term predictions about the behavior of the system.

The laws of nature have reflected the complete connection between cause and effect. Thus until recently, it was assumed that it was always possible to make accurate long-term predictions of any physical system so long as one knows the starting conditions accurately enough. This is very obvious for linear systems where the cause and effect connection is clear. In the case of nonlinear systems, the cause and effect connection can sometimes be not so simple. Thus the problem of controlling such a system arises. Although the systems that chaos theory deals with are complicated and most of the time unpredictable, the basic concepts of chaos are not very difficult to understand. Now comes the question of how chaotic systems manifest themselves. A system can show a multiple periodicity or apparent broadband noise as a result of an underlying chaotic dynamics. To qualify and quantify chaos there are several dynamical properties to be used. Fractal dimension of the reconstructed phase space of

the system, Kolmogorov entropy and Liapunov spectrum are most important of these dynamical properties.

The connection between chaos theory and everyday life involves the analysis of time series obtained from real systems. The difficulty arises from the projection of a multidimensional system on a scalar one dimensional time series. Linear methods interpret all regular structure in a data set which means that the intrinsic dynamics of the system are governed by the linear paradigm that small variations cause small effects. So all irregular behavior of the system should be a result of external random input. But from our knowledge of chaos theory, nonlinear, chaotic systems can produce very irregular data with purely deterministic equations of motion.

The theory of nonlinear dynamical systems provides new tools and quantities for the characterization of irregular time series. Some of these methods are summarized in Table 1.1.

Table 1.1. Characteristic differences of linear and nonlinear systems

Activity	**Linear**	**Nonlinear**
Finding the signal	Few Frequencies Seperate broadband noise from narrow band signal	Many frequencies Seperate broadband noise from broadband signal
Finding the space	Fourier analysis Univariate and multivariate statistics	Phase space reconstruction using delay variables and embedding dimensions.
Classify signal	Sharp spectral peaks, resonant frequencies. Quantities independent of initial conditions.	Invariants such as Liapunov Exponents, Fractal dimensions. Quantities independent of initial conditions.
Make models and predict	$x(n+1) = \sum c_n x(n)$	$x(n) \rightarrow x(n+1)$

Chaotic structures are very common in nature. From physics to biology, in micro or macro systems one can encounter nonlinear systems. Even very simple systems can show extremely complicated dynamics. Chaotic behavior can be seen in time dependent system as well as in three dimensional structures. Polymers as dielectrics are also known to exhibit chaotic behavior both in their structure and dynamics.

This work is on chaotic structures in the transient current through aluminum-polymethylmethacrylate-aluminum thin films [4]. Polymethylmethacrylate (referred to as PMMA in the rest of this work), with the formula $\left[-CH_2-\left(CH_3\right)C\left(COOCH_3\right)\right]_n$ is a polymer whose dielectric behavior has been studied [5, 6]. Data were taken according to the two standards ASTM-D257 and IEC93; both methods involve applying a potential diference to either side of a planar sample of dielectric and measuring the current flow. Hacınlıyan et. al. [4] has reported a chaotic behavior in the transient current through PMMA. That report was based on a single observation and the reproducibility of the chaotic behavior was not analyzed. The dependence of the transient current on the temperature and the applied field was also lacking. This work continues this earlier report on signs of chaotic behavior observed in the time dependent, transient behavior of the current across a thin film of PMMA with regard to reproducibility and behavior under different voltages and at different temperatures. The reproducibility of the behavior ensures that the chaoticity does not stem from an experimental error. The transient current in Al-PMMA-Al thin films for times in the range of ten thousand seconds to ten hours has been analyzed. Several sets of data on different samples were taken at intervals of 1s, 5s, 10s and 20s using a range of different voltages at a fixed temperature, 303 K and subsequently under a range of different temperatures at a fixed voltage of 10 V.

The experiment was originally designed for finding the steady state value for the current in an attempted study of conductivity mechanisms in PMMA samples. The relatively peculiar behavior of the observed transient current and the unusually long times required for reaching a possible steady state implied the alternative of chaotic behavior. Polymeric dielectrics are known to be very sensitive to their thermal, mechanical and electrical history [5, 6]. They also contain many impurities and additives.

The difficulty of obtaining identical results under nearly identical conditions is well known in the literature [5]. Polar polymers such as PMMA, are known to need very long times to achieve steady state current. From theoretical considerations [6], this time is estimated to be approximately a hundred years for PMMA and it becomes necessary to understand the observations by other nonlinear considerations.

It is also known that below the glass transition temperature beta relaxation process takes place in PMMA. Broad relaxation times are related to the interaction of the molecular chain parts which have dipole moments, with the electric field. Thus, at room temperatures the time dependence of the conductivity can be described by a beta type of dipole relaxation polarization [6]. Our aim is to consider the transient current as a time series semi- empirically and study possible chaotic behavior in the transient conductivity mechanism of PMMA. In general after the application of voltage, the current falls off with fluctuations (polarization current) and only after a long delay seems to become steady. The processes that are suggested to explain this behavior of the current are slow types of dipole relaxation, polarization, trapping of charge carriers, electrode polarization due to complete or partial electrode blocking and conduction current generated by thermal ionization of impurities.

It is observed that the chaoticity is inherent, and is a reason for the observed behavior that appears to differ somewhat under nearly identical conditions (identical temperature, voltage, humidity, illumination etc.) since very similar chaotic behavior has been observed under these apparently different conditions. Furthermore, the observed chaotic behavior persists for a wide range of values of the temperature and the external field. Hence the dynamics underlying the transient current can be understood in terms of chaoticity.

Another aspect of this work was to find a theoretical model which can explain the conductivity mechanism of PMMA at least qualitatively. The non-exponential behavior of the transient current and the randomness of the impurities in PMMA suggests the charge density wave model. This model supplies a good theoretical environment to study the quenched random potentials due to impurities and the non-exponential

relaxation of the transient current at the same time [7]. The simulated polarization current of the pinned charge density wave shows a stretched exponential behavior [7]. So we fitted the transient current to a stretched exponential function and obtained satisfactory results. The direct fit of the data to the charge density wave model gave also promising results but needs further exploration because of technical difficulties.

The plan of the thesis is as follows: In chapter two, theoretical background on the nonlinear time series analysis methods used in this study is given. In chapter three, the implementation of the nonlinear methods to the data is shown and the results are tabulated. In chapter four, the pinned charge density wave model is introduced and qualitative agreement between the data and simulations are presented. In chapter five, conductivity mechanisms in polymers are briefly explained. The results of the chaotic exploration of the data and their connection with the conductivity mechanisms are given. Chapter six contains the conclusion of this study.

2. NONLINEAR ANALYSIS OF TIME SERIES

Chaos occurs from the nonlinear evolution of systems which are governed by either differential equations in the form of

$$\frac{dx}{dt} = F\left(x\left(t\right)\right) \tag{2.1}$$

or non-invertible discrete time maps

$$x\left(t+1\right) = F\left(x\left(t\right)\right) \tag{2.2}$$

involving three or more degrees of freedom in differential form and two or more degrees of freedom for the map form $x\left(t\right) \in R^n$ discribes the dynamical state of the system. Chaos can be recognized from the orbits $x\left(t\right)$ as complex time traces with continuous, broadband Fourier spectra, non-periodic motion, and exponential sensitivity to small changes in the trajectory. In the sense of time series one has only scalar measurements at hand from which one can understand the dynamical mechanism of the system. But to extract quantitative information from the scalar time series one has to go from scalar observations to the phase space of the dynamical system where chaotic motion takes place. Phase space reconstruction is the solution to this problem.

2.1. Phase Space Reconstruction

The embedding theorem [8, 9] is used to convert scalar observations to vectors in the phase space. From the theorem it follows that the m-dimensional delay embedding space is equivalent to the original unobserved phase space of the underlying dynamical system. To reconstruct the phase space from the scalar transient current $s\left(k\right)$, we have to form the vectors $\vec{y}(k)$ given by

$$\vec{y}(k) = \left(s\left(k\right), s\left(k+\tau\right), ..., s\left(k+(d-1)\tau\right)\right) \tag{2.3}$$

where τ denotes the delay time and d denotes the embedding dimension. The equation above replaces the scalar measurement with the new data vectors in Euclidean d-dimensional phase space. Here the information of the invariants of the original system is conserved. This means that this new reconstructed phase space allows us to investigate all the invariants of the original system as if they were evaluated in the original space. As stated in the theorem the embedding dimension does not need to be the same as the original phase space of the system. But to minimize the calculations one has to determine an optimal dimension. Another problem arising with the phase space reconstruction is what delay time to use. In theory all the time lags are equivalent. But in practice, to identify the deterministic structure of the time series a suitable time lag should be chosen. It is very natural to take time delay as a multiple of the sampling time of the time series. If time delay is taken too short then newly constructed vectors will not be independent enough. And this will cause loss of some information about the original system. On the other hand if we choose a too long delay time than the measurements will appear to be random because of the chaotic nature of the system [11]. There are a number of linear and nonlinear tools to choose a suitable delay time and an embedding dimension, that we now present.

2.1.1. Average Mutual Information

The method of time delayed mutual information is a tool to determine a suitable time delay [12, 13]. The mutual information between measurements a_i drawn from a set $A = \{a_i\}$ and measurement b_j drawn from a set $B = \{b_j\}$ is the amount learned by the measurement of a_i about the measurement of b_j . The mutual information function S is given by,

$$S = -\sum_{ij} p_{ij}(\tau) \ln \frac{p_{ij}(\tau)}{p_i p_j}. \tag{2.4}$$

Here p_i is the probability of finding a data value in the i-th interval. $p_{ij}(\tau)$ is the joint probability of data to be in the i-th interval first and τ times later in the j-th interval. Mutual information gives a notion of information connection between the data values.

The first minimum of the average mutual information versus τ gives a good estimate for the time delay [14].

2.1.2. Autocorrelation Function

Another statistical method to determine a suitable time delay is to look at the autocorrelations of a signal. It is given by

$$c_\nu = \frac{1}{\sigma^2}\langle (s_n - \langle s\rangle)\,(s_{n-\nu} - \langle s\rangle)\rangle = \frac{\langle s_n s_{n-\nu}\rangle - \langle s\rangle^2}{\sigma^2} \tag{2.5}$$

where

$$\langle s\rangle = \int_{-\infty}^{\infty} ds' s' p(s) \tag{2.6}$$

and $p(s)$ is the probability density function.

$$\sigma^2 = \langle (s - \langle s\rangle)^2\rangle = \int_{-\infty}^{\infty} ds' (s' - \langle s\rangle)^2 p(s') \tag{2.7}$$

s_n is a measurement taken at time step n. The distribution of data values can be identified with the use of autocorrelation. If the autocorrelation function is zero then we can conclude that the data points are distributed evenly over the space. In other words, $s(n)$ and $s(n-\nu)$ are independent enough to be used as coordinates in a time delay vector, but also carry enough information about the connection between them. So the first zero crossing of autocorrelation function gives another clue about the time delay value to use [11].

2.1.3. The False Nearest Neighbor Method

After choosing a suitable time delay, the question of choosing an embedding dimension arises. In the case of time series, as we mentioned before, the phase space of a system is projected onto a lower dimensional space. Therefore, a good embedding dimension is very crucial to distinguish the observed orbits from self overlaps arising

from projection of the original phase space. From the embedding theorem, we know that if the box-counting dimension of the attractor is D_f, then an integer dimension d_E (embedding dimension) which is greater than $2D_f$ will sufficiently unfold the attractor in the reconstructed phase space. To reduce computational effort to a minimum, one needs a criterion for the minimum embedding dimension, sufficient to unfold the attractor. At this point the false nearest neighbors method [14] is a useful tool to give an estimate for the embedding dimension. Beginning with the reconstructed data vectors in d dimensions with a proper time lag τ, and the time delay vector

$$\vec{y}(k) = [s(k), s(k+\tau), ..., s(k+(d-1)\tau] \tag{2.8}$$

The nearest neighbor in phase space of the vector will be another time delay vector,

$$\vec{y}_{NN}(k) = [s_{NN}(k), s_{NN}(k+\tau), ..., s_{NN}(k+(d-1)\tau] \tag{2.9}$$

If $\vec{y}_{NN}(k)$ and $\vec{y}(k)$ are real neighbors then the relation between them must originate from the dynamics of the system. But if the chosen embedding dimension is not large enough then the attractor will not unfold properly and because of the projection, false data points will fall into each others neighborhood. Increasing the embedding dimension will decrease the number of false neighbors. One looks for the dimension at which all false neighbors are removed for each data point, by switching to the next higher dimension.

Definition of the neighborhood of a data point needs a criterion for deciding whether two points in dimension d are close or far in dimension $d+1$. When dimension is increased, an extra component is added to both vectors $\vec{y}_{NN}(k)$ and $\vec{y}(k)$, which are $s(k+d\tau)$ and $s_{NN}(k+d\tau)$. To decide if $\vec{y}_{NN}(k)$ is a true neighbor of $\vec{y}(k)$, one simply compares the distance between the vectors in d dimensions with the distance between them in $d+1$ dimensions. If the compared distances in dimension d and $d+1$ are comparable to each other than we have true neighbors. But if the distance in dimension $d+1$ is larger than the distance measured in dimension d then the neighbor of $\vec{y}(k)$ is said to be false. In Euclidean geometry this can be formulated as described

below:

In dimension d+1 the distance between the nearest neighbor points is:

$$R_{d+1}(k)^2 = \sum_{m=1}^{d+1} [s(k+(m-1)\tau) - s_{NN}(k+(m-1)\tau]^2 \tag{2.10}$$

which can be written in terms the corresponding distance in d dimensions $R_d(k)$ as

$$R_{d+1}(k)^2 = R_d(k)^2 + |s(k+d\tau) - s_{NN}(k+d\tau|^2 \tag{2.11}$$

The ratio of the distance between the neighbor points can be computed via,

$$\sqrt{\frac{R_{d+1}^2(k) - R_d^2(k)}{R_d^2(k)}} = \frac{|s(k+d\tau) - s_{NN}(k+d\tau|)}{R_d(k)} \tag{2.12}$$

When this ratio is larger than some chosen threshold value, the vectors are false neighbors.

Up to this point we have explained the tools to reconstruct the phase space. As this newly constructed phase space totally reflects the universal properties of the original phase space of the dynamical system, we can determine whether this system is chaotic or not. There are a number of dynamical properties which allow us to make this conclusion: Fractal dimension of the reconstructed phase space, Kolmogorov entropy and Liapunov exponents. We will use Liapunov exponents to identify the chaoticity of nonlinear time series.

2.2. Liapunov Exponents

Chaotic systems are very sensitive to initial conditions. This sensitive dependence on initial conditions and unpredictability comes from the nature of the chaotic system. The nearby trajectories diverge exponentially fast over time. This exponential divergence is a strong character of the chaotic systems. The averaged exponent of this

divergence is called the Liapunov exponent.

Let x and y be two nearby trajectories in d dimensional phase space. The time dependent evolution of their distance is given by

$$\begin{aligned} y_{n+1} - x_{n+1} &= F(y_n) - F(x_n), \\ &= J_n(y_n - x_n) + O(\|y_n - x_n\|^2 \end{aligned} \tag{2.13}$$

Here J_n is the $d \times d$ Jacobian matrix of F at a point. If the distance between x_n and y_n is known than one can compute this distance one time step later. If e_i is an eigenvector of J with eigenvalue Λ_i, then then the distance, δ_{n+1} can be written in the form of $\delta_{n+1} = \sum \beta_i \ \Lambda_i e_i$, where β_i is a stretching factor. So one can find as many stretching factors as there are phase space dimensions, that is, d different local Liapunov exponents can be found for a d dimensional phase space. If there is at least one positive Liapunov exponent, while the system is in a finite region of state space, then one can conclude that the system is chaotic [11]. In a time series analysis since a finite time series is analyzed it is guaranteed that the time delay vector space is finite. Another aspect of the Liapunov exponents is that they are invariant under smooth transformations.

To find the maximal Liapunov exponent of a time series, chose a point s_{n_0} with all its neighbors in the vicinity of ϵ. Compute the average over the distances of all neighbors to the reference part of the trajectory as a function of the relative time. The logarithm of the average distance at time Δn is some effective expansion rate over the time span Δn containing all the deterministic fluctuations due to projection and dynamics [15, 16]. So to find the maximal Liapunov exponent one has to compute:

$$S(\Delta n) = \frac{1}{N} \sum_{n_0=1}^{N} \ln \left(\frac{1}{|U(s_{n_0})|} \sum_{s_n \epsilon U(s_{n_0})} |s_{n_0+\Delta n} - s_{n+\Delta n}| \right). \tag{2.14}$$

The reference point s_{n_0} are embedding vectors. U is the neighborhood of s_{n_0} with diameter ϵ. The size of the neighborhood should be chosen such that it must be

large enough to contain at least a few neighbors and as small as possible to avoid missing a small periodic component. If the graph of $S(\Delta n)$ versus Δn shows a robust linear increase for some range, its slope gives an estimation for the maximal Liapunov exponent per time step.

3. NONLINEAR ANALYSIS OF TRANSIENT CURRENT IN PMMA

The aperiodicity and broadband nature of the transient signal (see Figures 3.1, 3.2 and 3.3) inspired the idea of applying nonlinear time series analysis on the current. This required a phase space reconstruction and analysis. The current observed in these measurements is investigated via nonlinear time series analysis as described in the previous section and using TISEAN software package [14, 17].

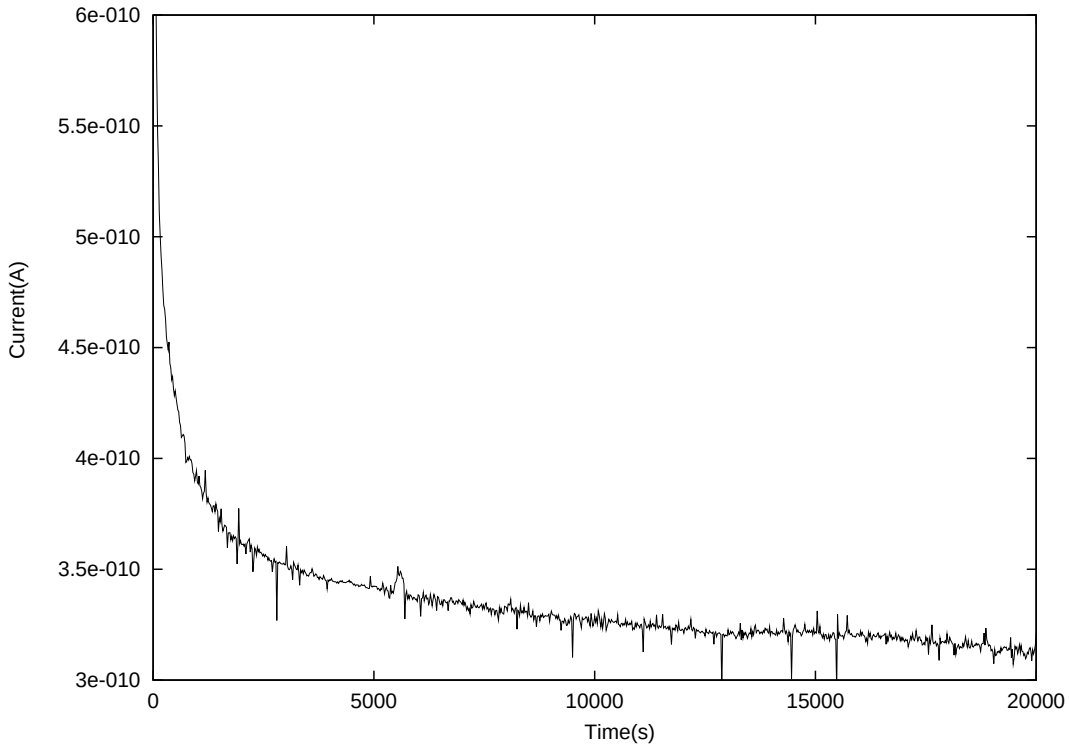

Figure 3.1. A typical transient current at room temperature at 10V

3.1. Experimental Setup

The specimens under investigation were prepared as sandwiched metal-polymer-metal structures with PMMA as the isolating layer. 300 nm thick aluminum electrodes were thermally evaporated at 10-6 mbar on microscope glass slides cleaned in a deter-

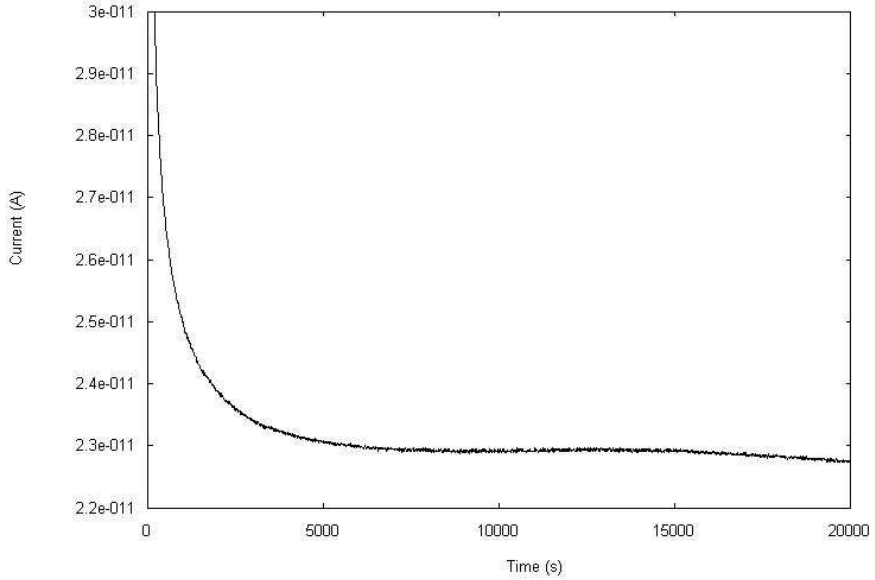

Figure 3.2. Transient current at 30C at 10V

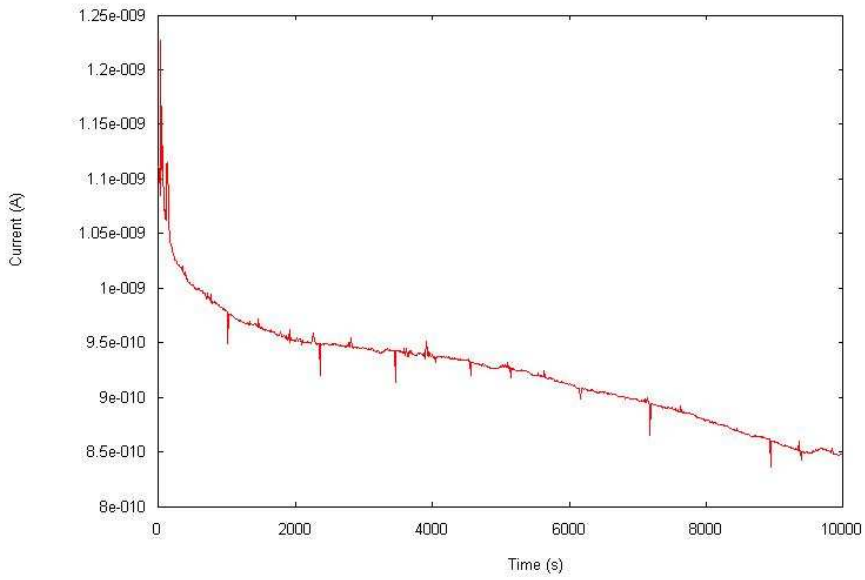

Figure 3.3. Transient current at 60C at 10V

gent solution . 20 μm thick PMMA layers were deposited from 6% PMMA solution in toluene. Subsequently, aluminum top contacts were evaporated. The I-V measurement was performed via programmable picoammeter/voltage source (Keithley, model 487) and a temperature controller (Lake Shore, model 300). The picoammeter and the temperature controller were interfaced to a computer through an interface card that automated data taking, as shown in Fig.3.4.

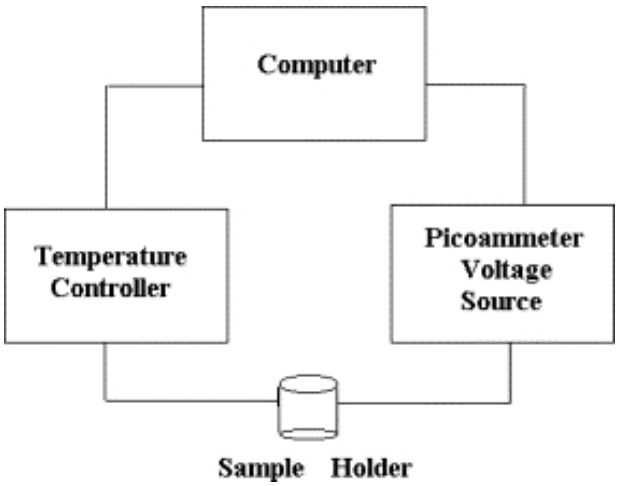

Figure 3.4. Experimental Setup

The picoammeter model 478 used is capable of reading currents in the range 10 fA to 2 mA. It also serves as a DC voltage supply in the range $\pm 500V$. In an I-V measurement a given voltage range $V_{\min}$ to $V_{\max}$ is scanned by constant increments V at constant time intervals Δt. ΔV and Δt are controlled by the computer in the following manner;

- The computer drives the voltage supply to apply the lower voltage limit $V_{\min}$ to the sample and to wait for a prescribed time in order to let the current settle down.
- When 9/10 of Δt elapses, the current values are averaged over very short time intervals with respect to time interval Δt.
- At the end of Δt seconds, the voltage and the corresponding averaged current value for the last one tenth of Δt are recorded in the output file. Then the voltage is incremented by ΔV.
- The procedure is applied repeatedly until the voltage reaches $V_{\max}$.

When a DC voltage is applied, the current in the system achieves a stationary state only after a definite time [18]. With the same setup, the extent of the settling time Δt is determined by applying a small voltage on the sample and then recording the time evolution of the resulting current. Strong fluctuations that saturate in a time scale around 9000 s have been observed. A typical plot of the transient current against time

can be seen in Figures 3.1 and 3.2. It can be seen that the transition region shows a typical pattern that can be associated with chaotic behavior in the context of pinned charge density waves as first reported by Erzan et al [7].

3.2. Choosing Time Delays

The real time data is finite and contains noise. Both noise and finiteness are obstacles to access infinitesimal length scales. So a reasonable choice of delay time is important to unreveal the underlying dynamics. Small delays will yield strongly correlated vector elements. The components of the vectors will become uncorrelated and randomly distributed in the embedding dimension if one chooses a large scale. To determine the time delay, as mentioned in chapter (2) one has to find first local

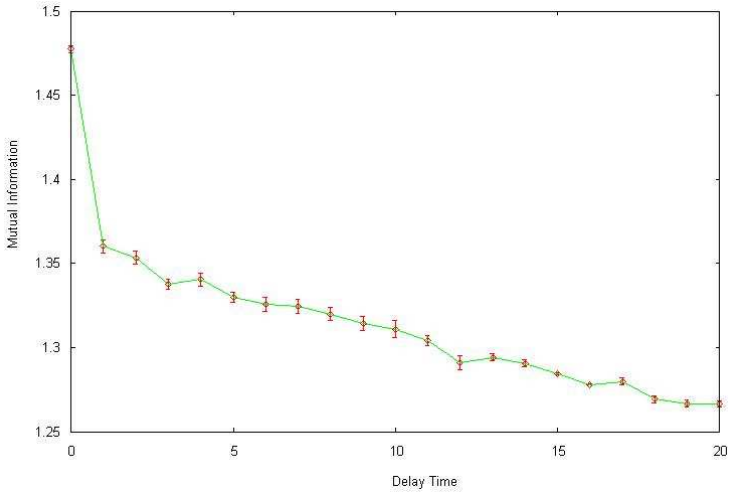

Figure 3.5. Average mutual information versus time delay for current at 30C under 10V

minimum of average mutual information (see Figures 3.5, 3.6 and 3.7) and/or the zero crossing of the linear autocorrelation function(see Figures 3.8, 3.9 and 3.10). The autocorrelation function gives values from 200 to 2000 units, whereas first local minimum of the average mutual information function gives values ranging between 2 to 200 units. The systematic error source is the picoammeter with a relative error of 1% . Hysterisis effect in polymers account for an observed random error in the range of 5% that has been propagated to the fits using the MINOS error analysis routine in MINUIT. The errorbars are obtained with error propagation method described in [10]. The time

delay chosen from average mutual information is more reliable because it also takes into account the possible nonlinearity. [11]. These two different time scales can be

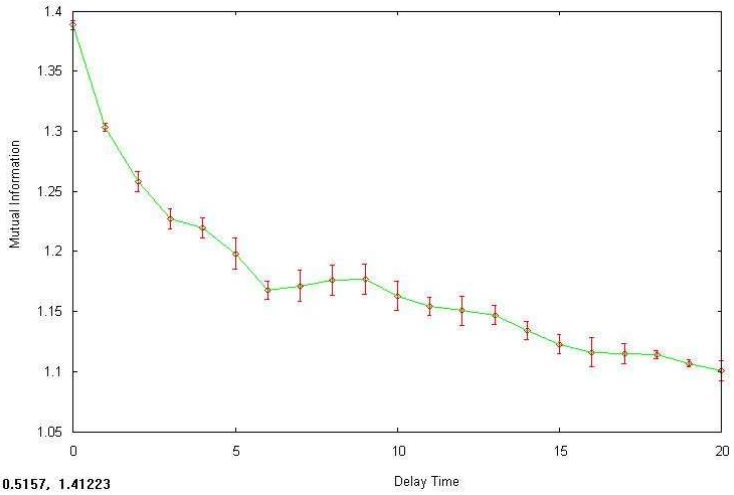

Figure 3.6. Average mutual information versus time delay for current at 30C under 30V

explained in the following manner. When nonlinearity is considered the current forgets its state approximately in 40s. But it is linearly correlated up to 20000s. This can be interpreted as two mechanisms which lead to two time scales. One is the long term transition to a steady state, the other is related to the aperiodic behavior during this transition. The average mutual information function and autocorrelation function

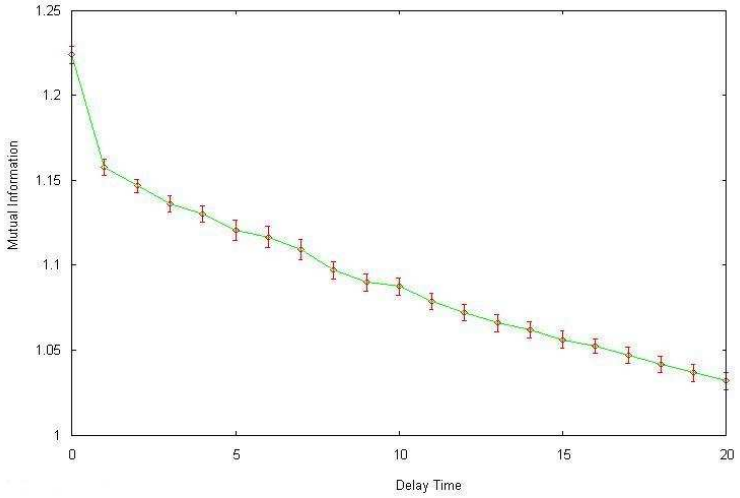

Figure 3.7. Average mutual information versus time delay for current at 30C under 50V

suggest different delay time. This values can be inspected visually by looking at the

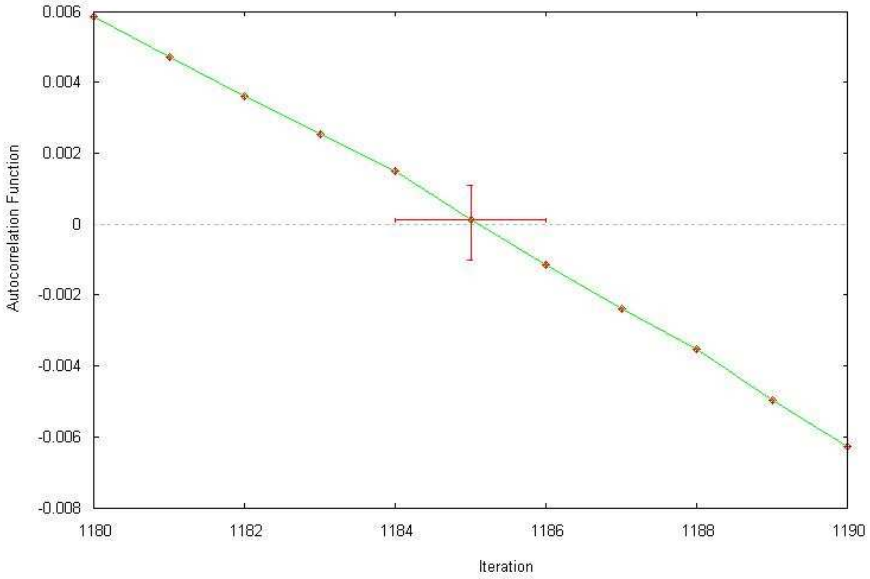

Figure 3.8. First zero crossing of autocorrelation function for current at 30C under 10V

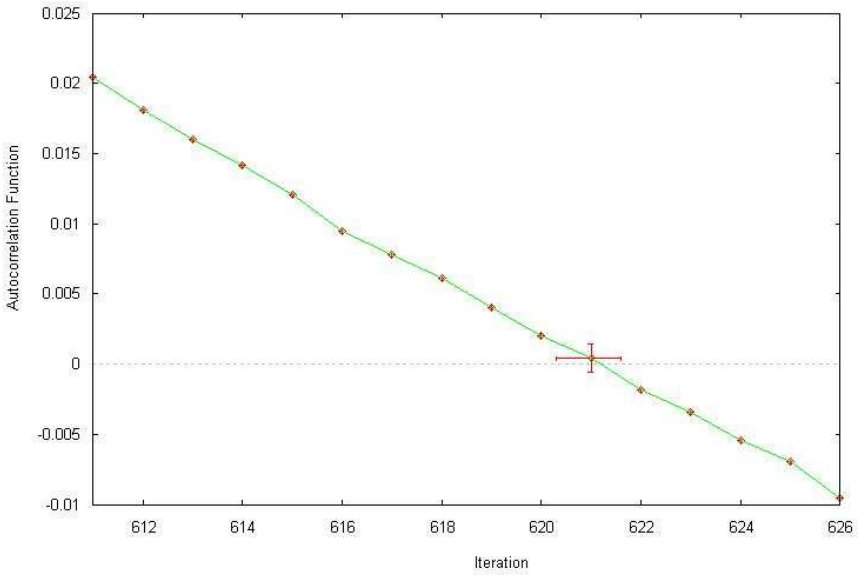

Figure 3.9. First zero crossing of autocorrelation function for current at 30C under 50V

time delay representation of the data. This inspection gives a notion whether the chosen delay time can unfold the attractor or not.

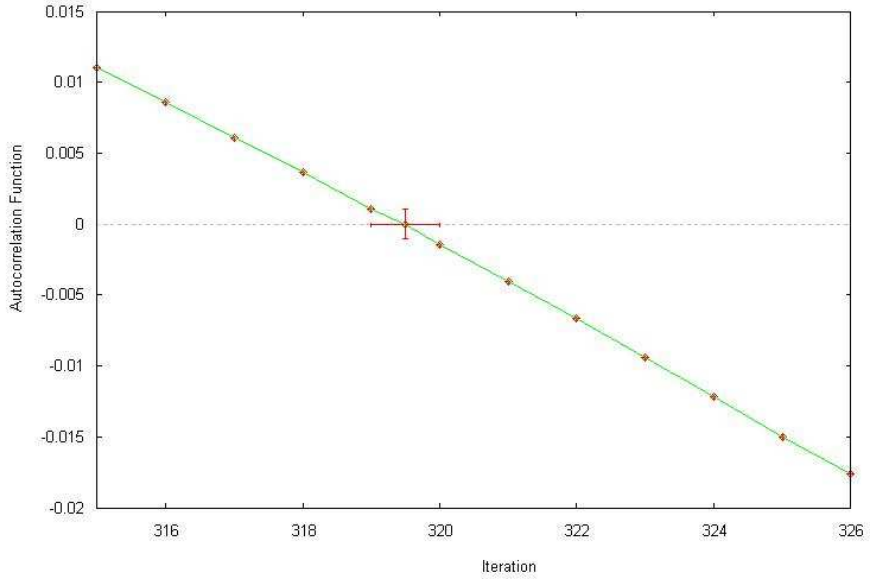

Figure 3.10. First zero crossing of autocorrelation function for current at 30C under 70V

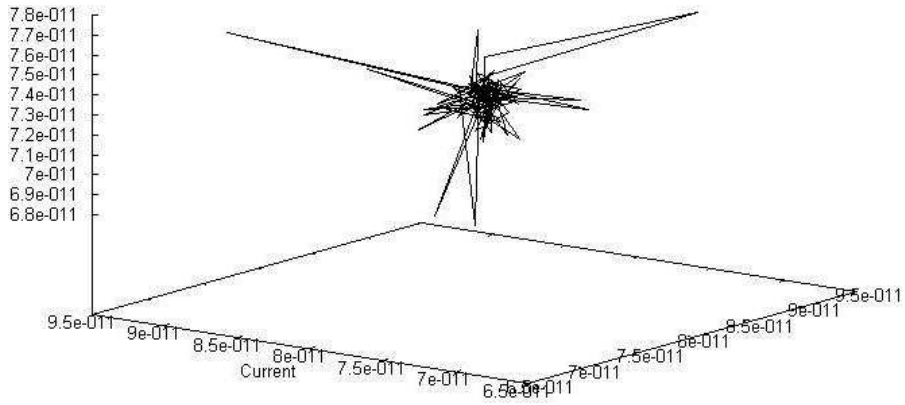

Figure 3.11. The time delay representation of the current at 30C and under 10V. Delay time of 20 is used

3.3. Choice Of A Suitable Embedding Dimension

Knowledge of a satisfactory embedding dimension is necessary to minimize computational effort. But if the embedding dimension is chosen too large this will add redundancy to chaotic data and thus will adversely affect the computation of Liapunov exponents [19]. To find a satisfactory value for the embedding dimension, false nearest neighbors method provides a good estimate. The fraction of false nearest neighbors are calculated. In Figures (3.12, 3.13 and 3.14) the fraction of false nearest neighbors versus embedding dimension are plotted. The ratio of the false nearest neighbors falls

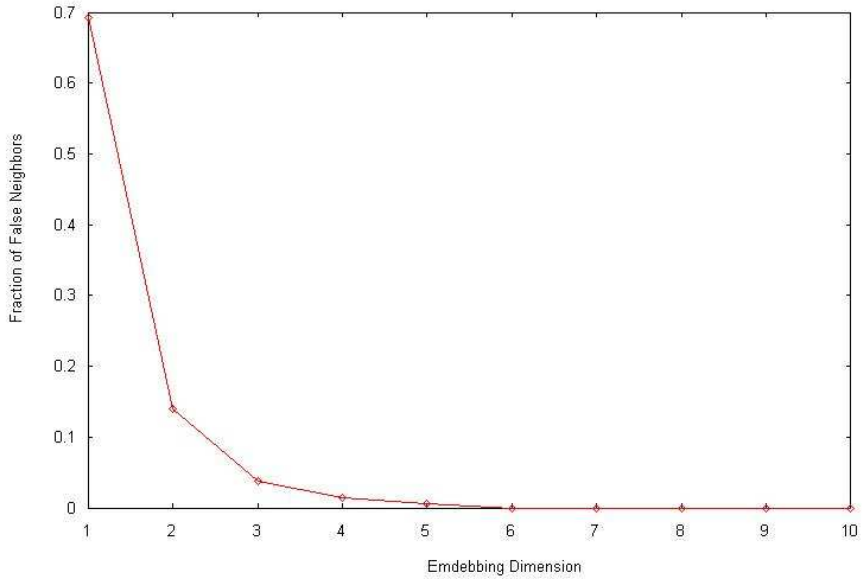

Figure 3.12. Embedding dimension versus false neighbors for current at 30C under 10V

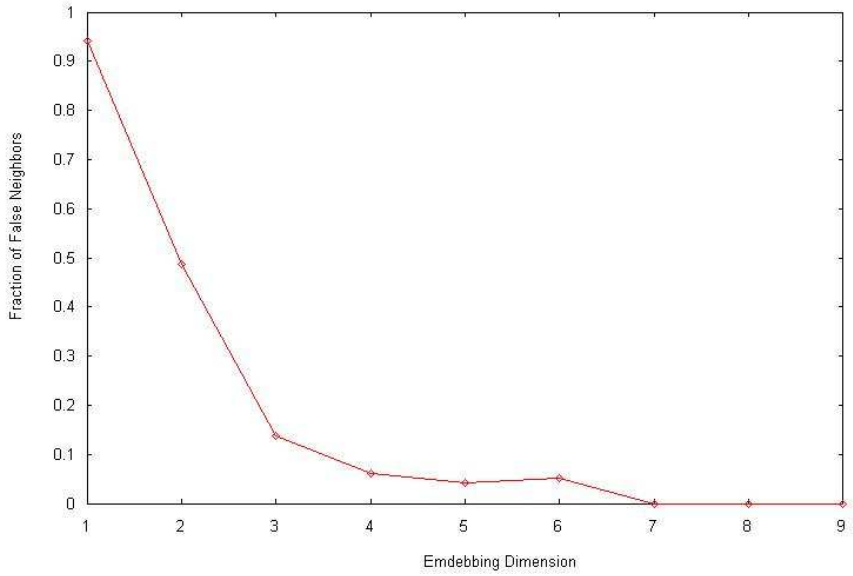

Figure 3.13. Embedding dimension versus false neighbors for current at 50C under 10V

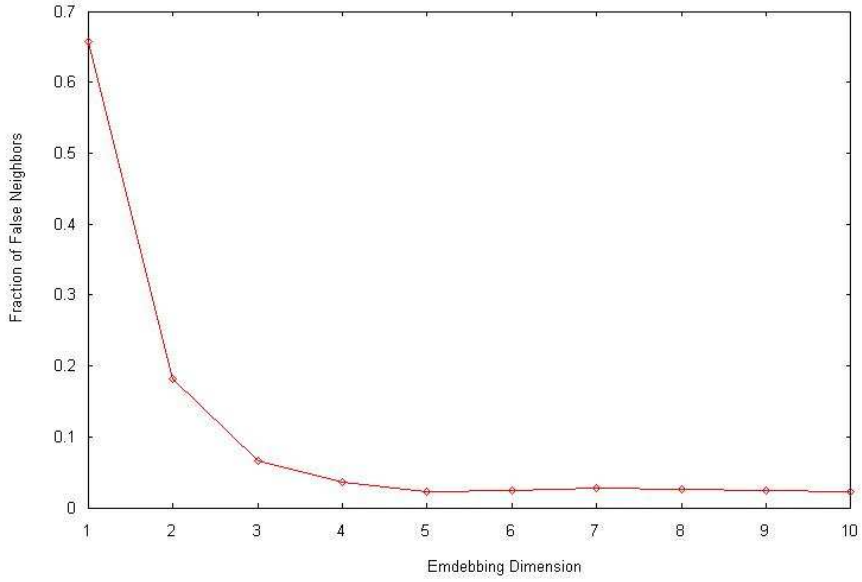

Figure 3.14. Embedding dimension versus false neighbors for current at 70C under 10V

drastically after embedding dimension three. So we can choose four as the embedding dimension safely for reconstructing the embedding space.

3.4. Maximal Liapunov Exponent

The Liapunov exponents are invariants of the dynamics. So they should not change if the dimension of the reconstructed state space is larger than the actual dimension of the state space. The maximal Liapunov exponents are estimated with the use of algorithm based on (2.15) coded as the lyapk routine in the TISEAN package[5, 6].

A sample of stretching factor versus iteration graphs for various temperatures and voltages are given in Figures 3.14, 3.15 and 3.16. The distinct curves correspond to different neighborhood sizes. The calculated values for different currents are given in Table 3.1. We see that irrespective of the choice of the stretching factor for different temperature and applied potential differences, a positive Liapunov exponent is indicated.

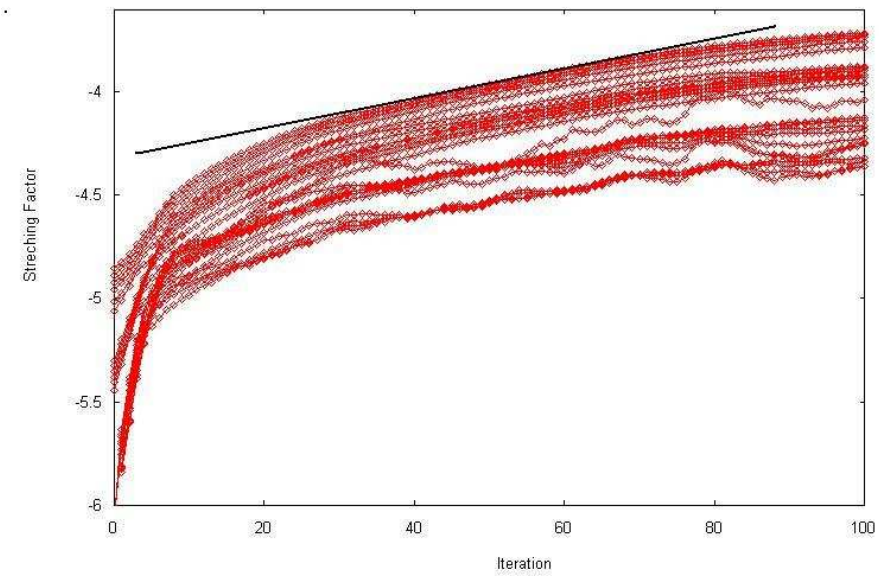

Figure 3.15. Streching factor versus iteration for current at 30C under 20V

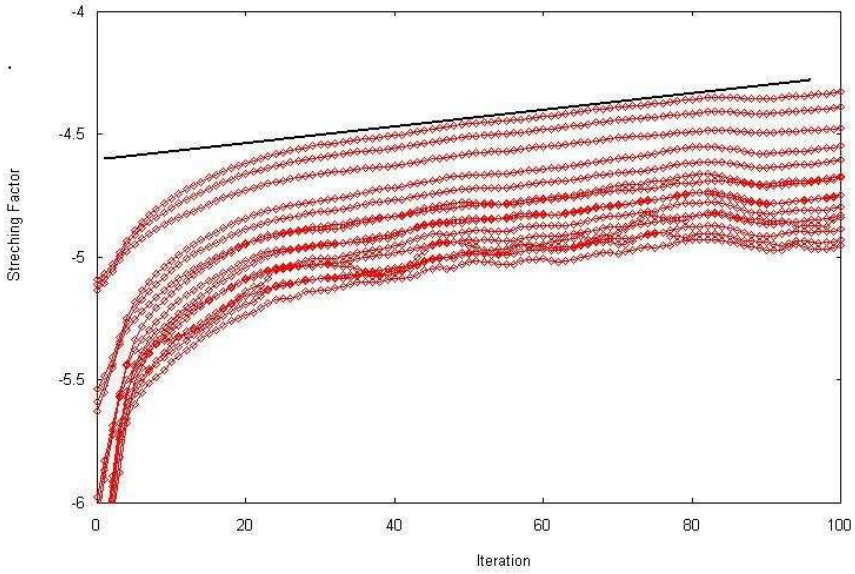

Figure 3.16. Streching factor versus iteration for current at 30C under 40V

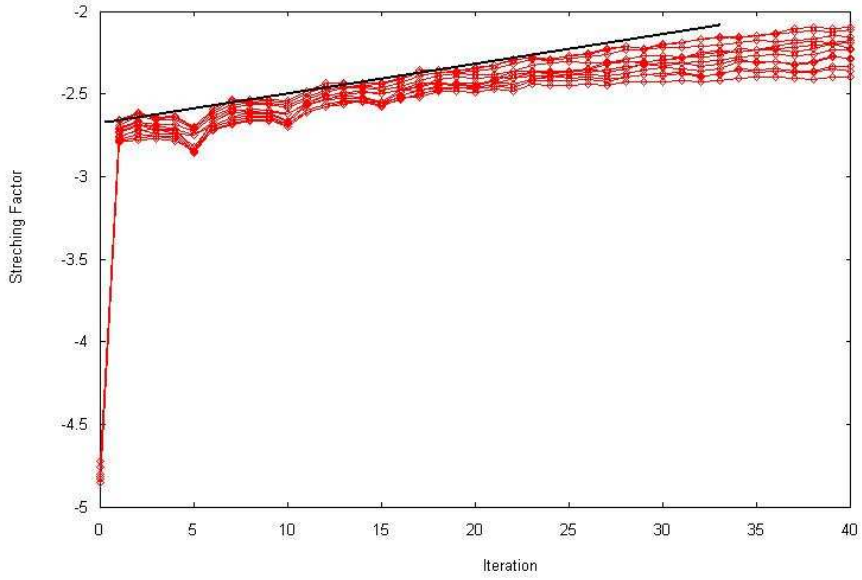

Figure 3.17. Streching factor versus iteration for current at 30C under 70V

Table 3.1. First local minimum of mutual information, zero crossing of autocorrelation function and maximum Liapunov exponents

E Field	Mutual Inf	Autocorrelation	Max. Liapunov Exp (bit/iteration).
0.50 MV/m	30s	1186s	0.0032 ± 0.0001
1.00 MV/m	30s	522s	0.0065 ± 0.0005
1.50 MV/m	60s	509s	0.0150 ± 0.0007
2.00 MV/m	40s	1113s	0.0039 ± 0.0004
2.50 MV/m	380s	1246s	0.0084 ± 0.0002
2.75 MV/m	90s	549s	0.0115 ± 0.0007
3.00 MV/m	110s	638s	0.0135 ± 0.0001
3.25 MV/m	20s	1186s	0.0159 ± 0.0006
3.50 MV/m	400s	638s	0.0178 ± 0.0003
3.75 MV/m	80s	212s	0.0226 ± 0.0001
4.50 MV/m	140s	709s	0.0161 ± 0.0001

4. QUENCHED RANDOM DISORDER

The presence of impurities and defects in polymeric structures prevents these structures from exhibiting long-range order. The competition between quenched random field and the elastic restoring forces invoke a very complex dynamics. Charge density waves (referred to as CDW in the rest of this work) provide one of the very few systems where it is possible to study the effects of quenched randomness in such systems.

The one dimensional model we have used is based on the work of Erzan et. al.[7]. The charge density wave is taken in the form

$$\rho(x) = e\rho_0 \left[1 + C\cos\left(q_0 x + \phi(x)\right)\right] \tag{4.1}$$

where ρ_0 is the one dimensional electron density, e is the electronic charge and q_0 is the wave number of the charge density wave. The phase $\phi(x)$ gives the position of the CDW. In a Peierls system C is defined as

$$C = \frac{N_0 \Delta}{a\lambda\rho_0} \tag{4.2}$$

where N_0 is number of sites, a is the lattice constant, λ is the electron phonon coupling and 2Δ is the gap. The energy density of the CDW is given by,

$$U = \frac{K}{2q_0^2}\left(\frac{\partial\phi}{\partial x}\right)^2 - \frac{e\rho_0}{q_0}\phi E + V_0 \sum_j \rho(x)\,\delta\left(x - x_j\right). \tag{4.3}$$

where K is defined as,

$$K = \rho_0 m_e v_F^2 \tag{4.4}$$

for a Peierls system [20]. Here m denotes the free electron mass, v_F is the Fermi velocity and E is the external field. The first term in the energy density equation gives the elastic energy of the CDW, and the second term is the coupling of the external field with the CDW. The third term involves the interaction enegy with impurities which are located at random positions x_j ($j = 1, ...,$ number of impurity sites). V_0 denotes the intensity of this interaction. If a damping force F_d, given by

$$F_d = -\frac{\rho_m}{q_0^2 \tau} \sum_j \dot{\phi}(x)\, \delta(x - x_j) \tag{4.5}$$

acting only at the impurity sites is introduced, the total equation of motion can be expressed as,

$$-\frac{K}{q_0^2}\frac{\partial^2 \phi}{\partial x^2} - \frac{\rho_m}{q_0^2 \tau} \sum_j \dot{\phi}(x)\, \delta(x - x_j) + e\rho_0 C V_0 \sum_j \sin(q_0 x_j + \phi(x))\, \delta(x - x_j) - \frac{e\rho_0}{q_0} E = 0 \tag{4.6}$$

where ρ_m is the effective mass density of the CDW, τ is a parameter which is related to the dissipated energy from the moving CDW to the lattice. This equation can be further simplified if we introduce the following dimensionless variables.

$$\begin{aligned} E_0 &= C V_0 n_i q_0 \\ B &= \frac{2\pi K n_i}{e C V_0 \rho_0 q_0^2} \\ \tau_0 &= \frac{2\pi \rho_m n_i^2}{e C V_0 \rho_0 q_0^2 \tau} \end{aligned} \tag{4.7}$$

The distance is taken to be $n_i x$, the time is scaled as t/τ_0 and the applied field is taken to be $\mathbf{E} = E/E_0$. Furthermore if we take $\Psi_i = \phi(x_i)/2\pi$, the equation of motion for the phases Ψ_i at each impurity site i, $i = 1, ..., N$, becomes,

$$\frac{d\Psi_i}{dt} = B\left[\frac{\Psi_{i+1} - \Psi_i}{r_{i+1} - r_i} - \frac{\Psi_i - \Psi_{i-1}}{r_i - r_{i-1}}\right] - \sin[2\pi(q r_i + \Psi_i)] + \frac{1}{2}\mathbf{E}(r_{i+1} - r_{i-1}) \tag{4.8}$$

In this equation random positions of the impurities are denoted by r_i and q is the wave number of the charge density wave. B and E are dimensionless constants which can be related to the diffusive coupling and the external field respectively. The equation of motion for the phases can be simplified by introducing the quenched random variables $\phi_i = qr_i$ where the values of ϕ_i range between 0 and 1, otherwise the distance between impurity sites are taken to be uniform.

$$\frac{d\Psi_i}{dt} = B\left[\Psi_{i+1} + \Psi_{i-1} - 2\Psi_i\right] - \sin\left[2\pi\left(\phi_i + \Psi_i\right)\right] + \mathbf{E} \tag{4.9}$$

(4.9) can be put into a form of recurrence relations for the values of Ψ_i by taking discrete time steps $t = n\delta t$ which then can be expressed as a set of diffusively coupled one dimensional maps.

$$\begin{aligned}\Psi_i\left(n+1\right) = &\left(1 - 2B\delta t\right)\Psi_i\left(n\right) - \delta t \sin\left[2\pi\left(\phi_i + \Psi_i\left(n\right)\right)\right] \\ &+ B\delta t\left(\Psi_{i+1}\left(n\right) + \Psi_{i-1}\left(n\right)\right) + \delta t\mathbf{E}\end{aligned} \tag{4.10}$$

This model is known [21] to exhibit sliding and a pinned phase for $\mathbf{E}$ values above or below a threshold value of an external field $E_{th}\left(B\right)$. Below the threshold value, a polarization $P\left(t\right)$ takes place due to the applied field[7] , which is related to the phases via,

$$P\left(t\right) = \frac{1}{N}\sum_i \Psi_i\left(t\right) \tag{4.11}$$

The polarization current, which is defined as,

$$J\left(t\right) = \frac{dP\left(t\right)}{dt} \tag{4.12}$$

exhibits a stretched exponential decay as $t \to \infty$ [7]. This behavior can be formulated as follows,

$$J\left(t\right) = a\exp\left(-bt^n\right) \tag{4.13}$$

where a, b and n are dimensionless constants.

4.1. Fit Of Data To Stretched Exponential Form

The nonlinear analysis of the transient current showed that the mutual information function and the auto- correlation function give two different time scales. The delay time obtained from the mutual information function was used to construct the reconstructed phase space. The time scale obtained from the autocorrelation function divides the data into two parts with two different regimes. The first part of the data contains the rapid fall of the current and a power law fit in the form of

$$I(t) = a \times t^{-b} \tag{4.14}$$

is used to interpret this part. For the second part we have used a modified stretched exponential form which is given by

$$I(t) = a \times t^{-b} \times \exp\left[-\left(\frac{t}{c}\right)^{n}\right], \tag{4.15}$$

where a, b, c and n are constants. The power law and the stretched exponential behavior can be found in various systems such as glasses [22], spin glasses [23]. We also know that the CDW model leads to a polarization current which exhibits a stretched exponential behavior [7]. The models used to explain the polarization currents will be given in the next section. To achieve a satisfactory fit we wrote a Fortran code which is given in Appendix A. We have also used the Mathematica software [24] to check the fits.

Our aim was to find the dependence of these parameters on temperature and applied field. These models give the qualitative behavior of the transient current. But the broadband nature of the current is suppressed and the fluctuations can not be explained quantitatively by these models. Some of graphs of the fit outputs are given in the following figures.

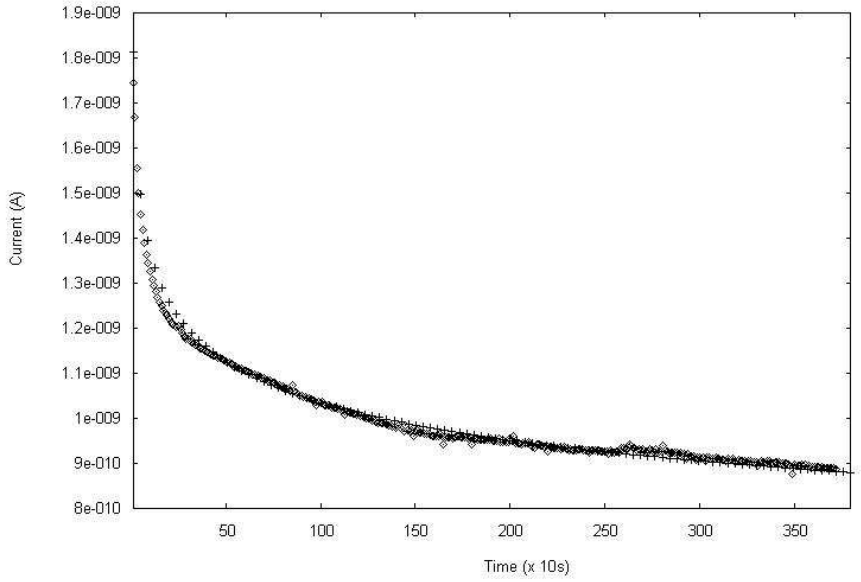

Figure 4.1. The power law fit(denoted by +) to the early stage of the current at 30C. a=1.8e-9 and b=0.121. The sum of the least squares is 3.8e-16. Applied potential is 10V

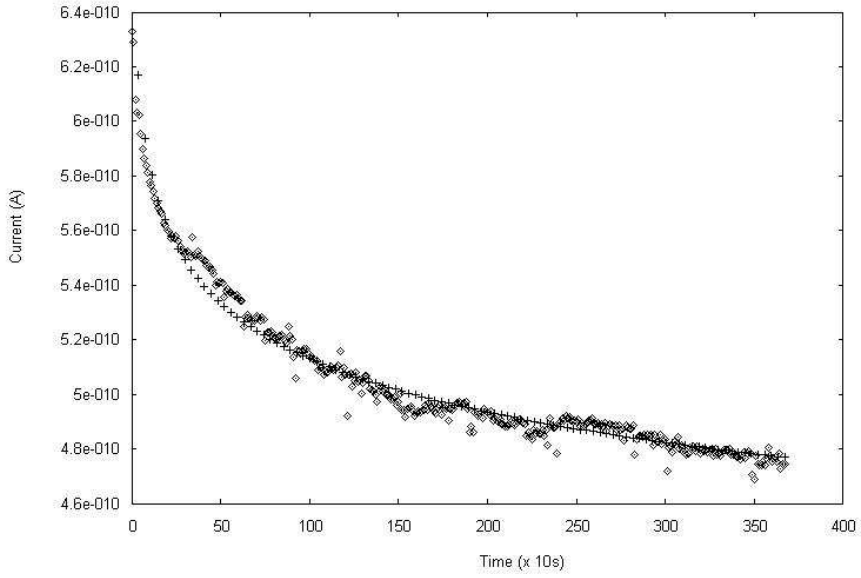

Figure 4.2. The power law fit(denoted by +) to the early stage of the current at 40C. a=6.64e-10 and b=0.06. The sum of the least squares is 9.41e-17. Applied potential is 10V

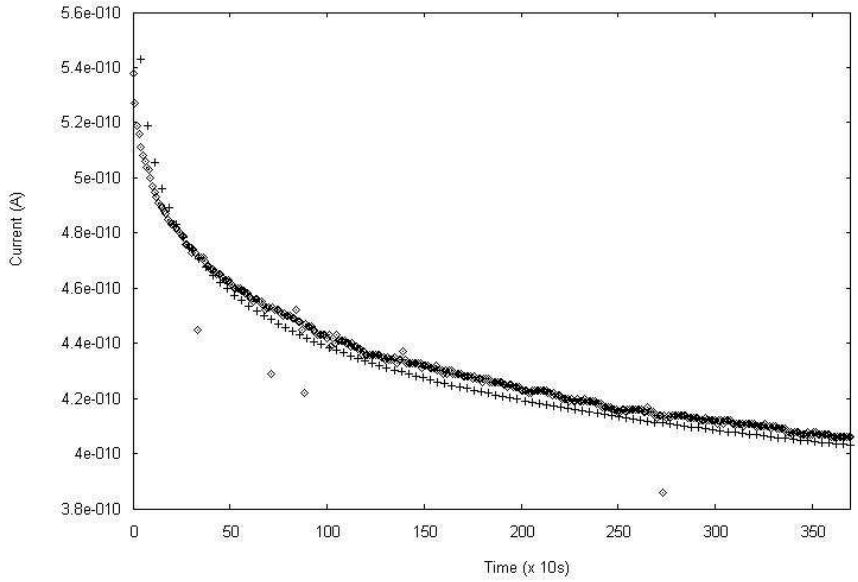

Figure 4.3. The power law fit(denoted by +) to the early stage of the current at 70C. a=5.9e-10 and b=0.06. The sum of the least squares is 1.64e-16. Applied potential is 10V

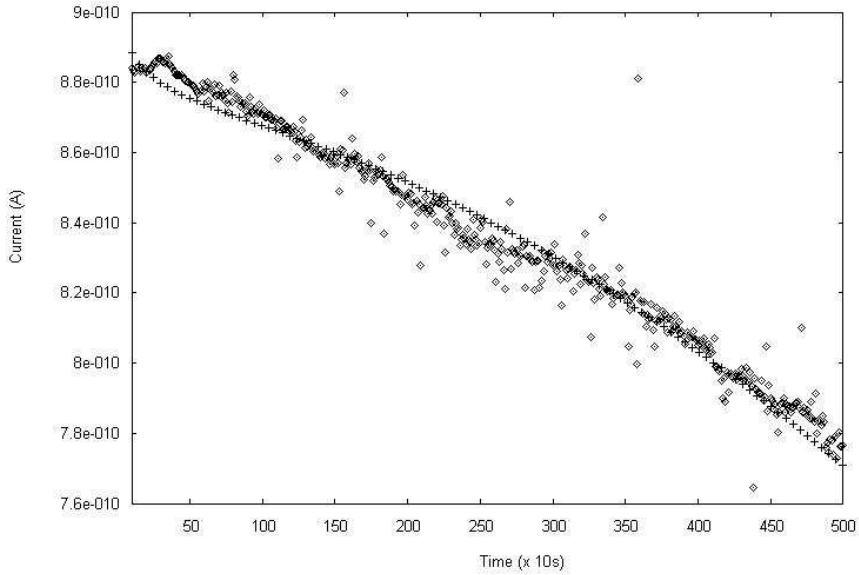

Figure 4.4. The stretched exponential fit(denoted by +) to the latter stage of the current at 30C. a=9.06e-10, b=0.008, c=1498 and n=2.02. The sum of the least squares is 4.21e-16. Applied potential is 10V

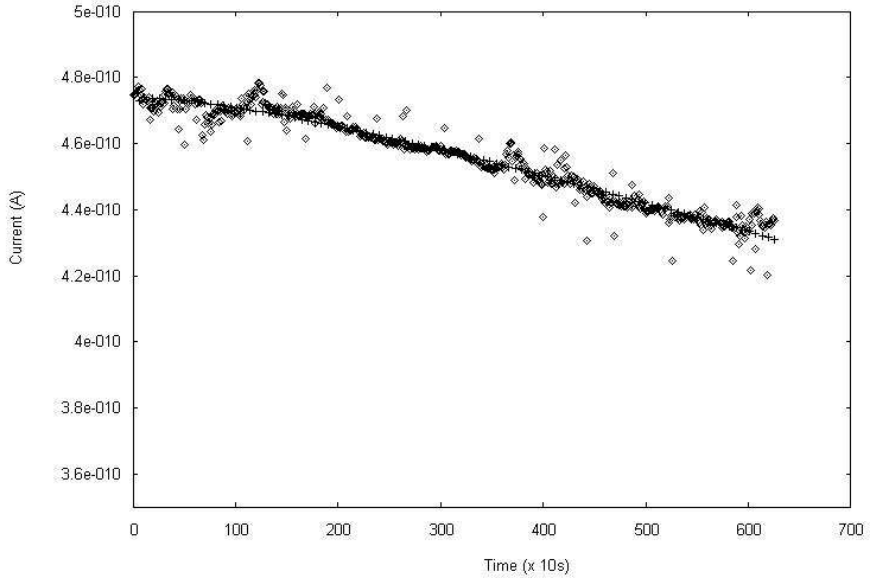

Figure 4.5. The stretched exponential fit(denoted by +) to the latter stage of the current at 40C. a=4.72e-10, b=0.002, c=3657 and n=1.30. The sum of the least squares is 1.3e-16. Applied potential is 10V

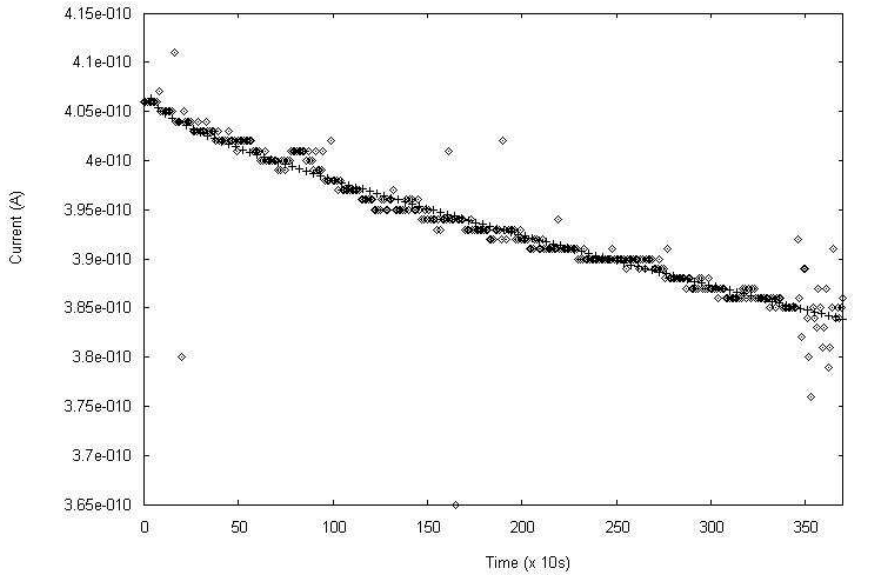

Figure 4.6. The stretched exponential fit(denoted by +) to the latter stage of the current at 70C. a=4.08e-10, b=0.002, c=9809 and n=0.93. The sum of the least squares is 9.53e-17. Applied potential is 10V

4.2. The CDW As A Model For The Transient Current Through PMMA

The recursion relation given by (4.10) can be numerically simulated, and with the use of the evaluated values of phases, one can compute the polarization current. Our first aim was to simulate the CDW model and then fit this model to the transient current through PMMA. The simulation and the fitting codes are written in the Fortran programming language. There are four parameters, the number of the impurity sites, the number of time steps, B value and E value that control the behavior of the CDW polarization current. Initial conditions are chosen randomly, that is, the code fills the initial values of the impurity sites with quenched random values which have values between 0 and 1. N (the number of time steps), E and B values are given manually to the code. The number of impurity sites is taken to be 10000. The changes in E and B values drastically changes the behavior of the simulated polarization current. In Figure 4.5 the polarization current with N=1000, B=0.987 and E=0.70 is given. As the parameter values are changed, the quantitative and the qualitative behavior of the polarization current changes. Some of the results of the simulations for different values of E and B are given in Figures 4.5, 4.6 and 4.7. The fitting part is more

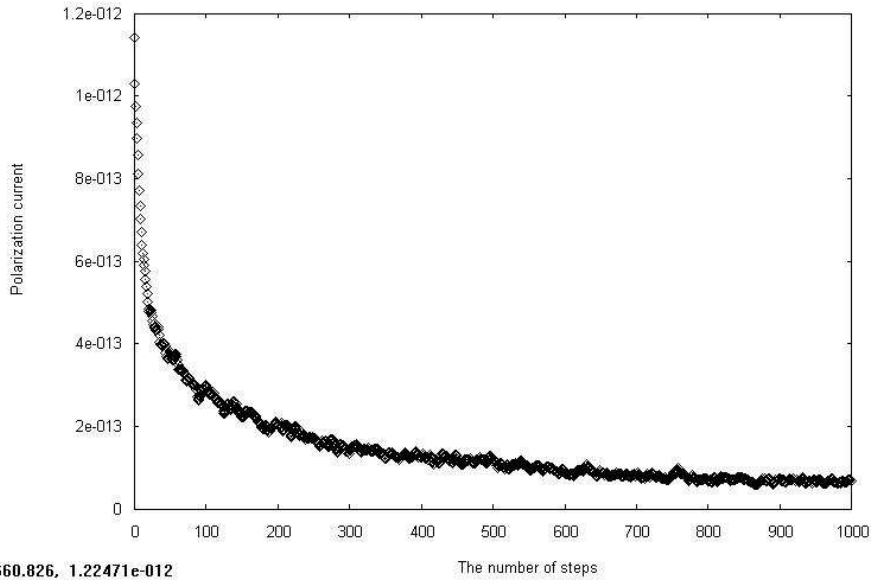

Figure 4.7. The simulated polarization current for E=0.70 and B=0.987. The number of time steps is taken to be 1000

problematic. The code reads the values of transient current and then tries to find

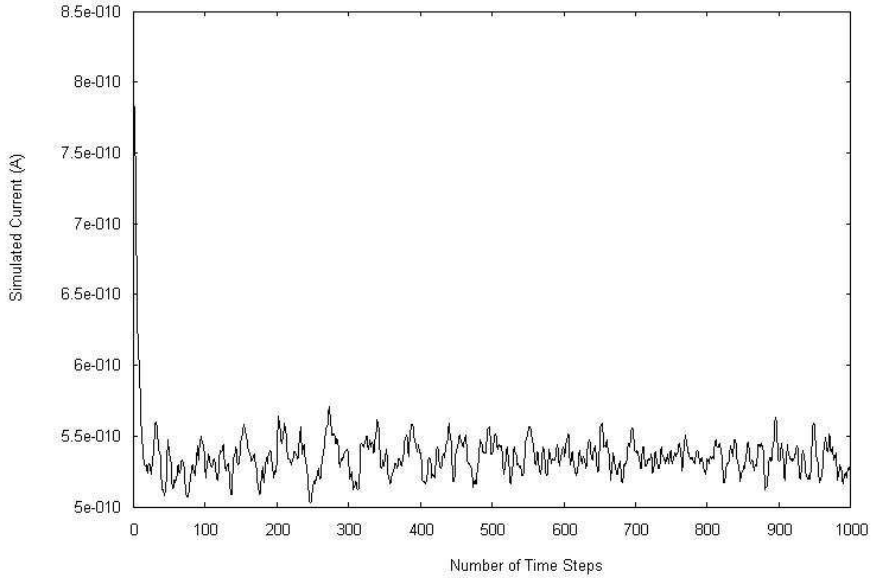

Figure 4.8. The simulated polarization current for E=0.71 and B=1.37. The number of time steps is taken to be 1000

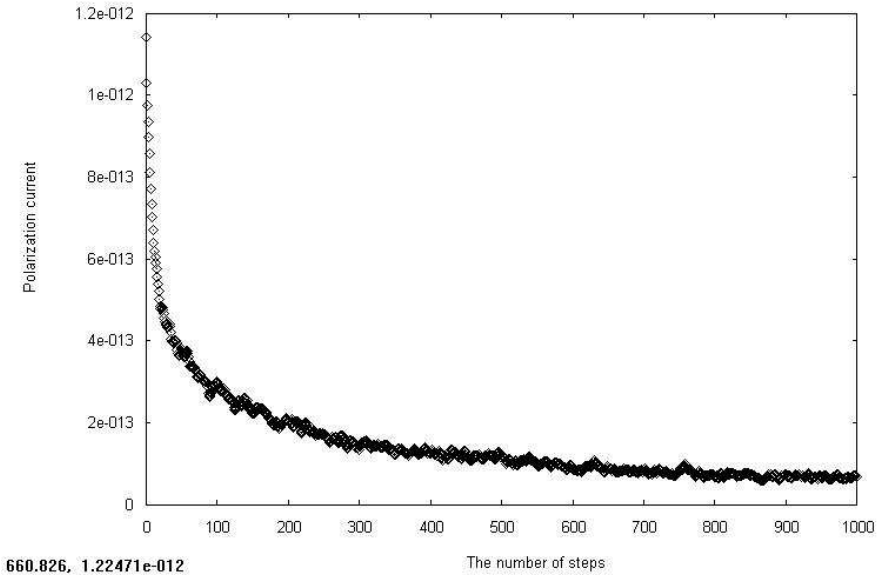

Figure 4.9. The simulated polarization current for E=0.70 and B=0.987. The number of time steps is taken to be 1000

values for E and B parameters that will fit the current to the CDW model. The minimization and error analysis of the fit is controlled by the MINUIT [25] package which is avaliable from CERN program library. MINUIT is a tool to find the minimum value of a multi-parameter function and analyze the shape of the function around the minimum. MINUIT returns E and B values for the given number of impurity sites. These E and B values are returned to the CDW simulation code. Every execution of the simulation code gives a current with different initial conditions. At this point there are two ways to average the obtained currents with fixed values of E and B. One way is to fix the number of impurity sites and then run the code to simulate currents. Each execution will begin with different initial conditions (as they are chosen randomly), hence will give quantitively different currents . Then the average is taken over these currents. The second way is more complicated and needs a very long computational time. In this case the number of the impurity sites is not fixed and the average is taken over the currents which have different number of impurities. We have used the first way in our simulations but the other option also gives interesting results. Sample graphs of fits are given in Figures 4.8 and 4.9. We have fitted the data for temperatures 20C to

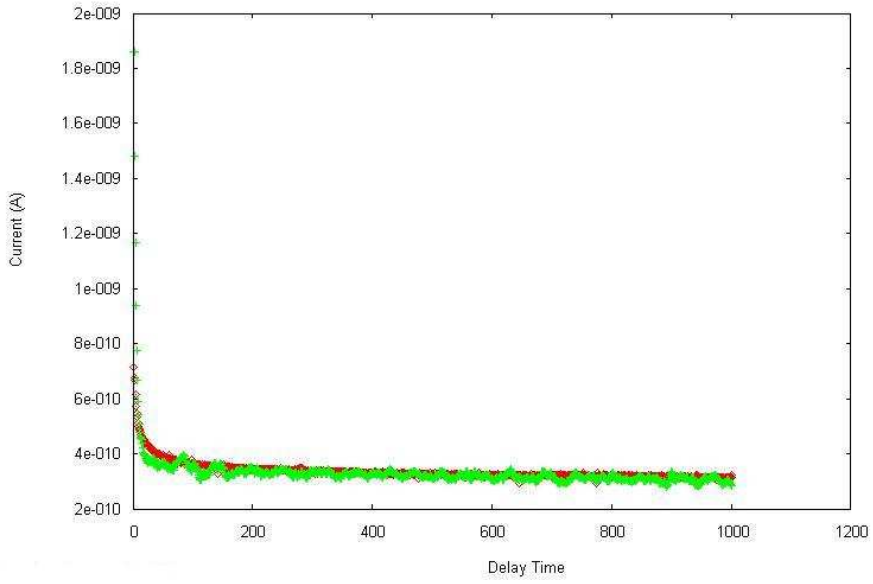

Figure 4.10. The CDW model fit(denoted by +) to the current at 30C under 10V. The estimated E and B values are 0.70 and 1.36 respectively

70C degrees under 10V. The E and B values versus the temperature is given in Figure 4.10.

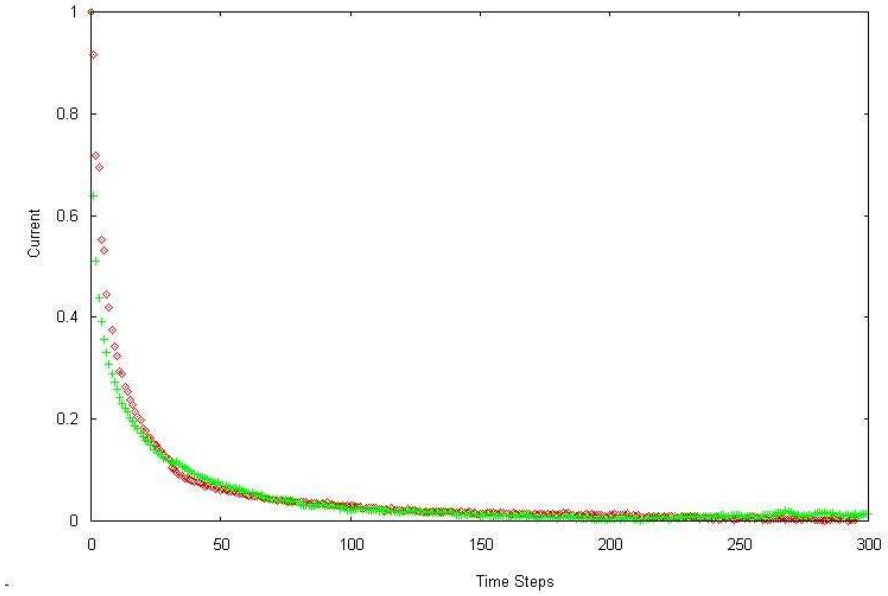

Figure 4.11. The CDW model fit (denoted by +)to the current at 30C under 20V. The estimated E and B values are 0.70 and 1.36 respectively. The current is normalized to unity for this case

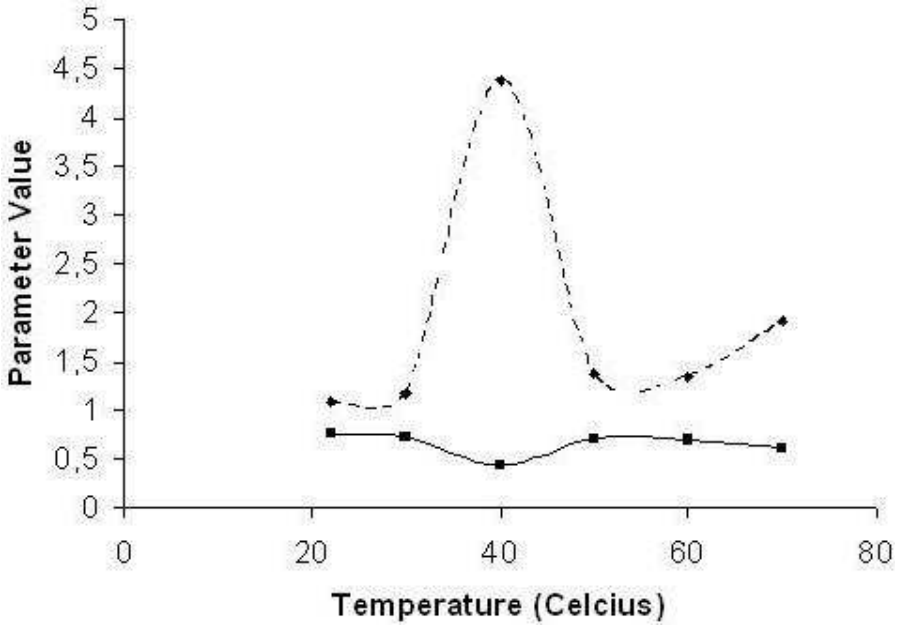

Figure 4.12. The variation of the E (the dashed line) and B values with temperature

4.3. Discussion

Our goal was to fit the data to the CDW model so as to explain the behavior of the transient current under the changes of the external parameters (especially the temperature and the applied electric field). The results are encouraging and gives clues of underlying dynamics.

The stretched exponential behavior of the transient current can be interpreted as a random walk between random sites. In [7], the dependence of the stretched exponential fit index on the external field is given. The behavior of the maximal Liapunov exponent versus the applied electric field from the PMMA data shows the same characteristics. This means that the maximal Liapunov exponent and the relaxation process are related.

There are two technical difficulties. One of them stems from the fact that, as we shall see in the next section, there are two or possibly three regimes and the overall normalization for these ranges deteriorates the quality of the fit. One can only fit either the short time behavior or the long time behavior with a single normalization constant, this is also in agreement with the fact that two different time scales have been observed via the correlation and mutual information functions.

The second difficulty is instability arising from the random orientation of sites and averaging over these random configurations as the parameters are varied. This affects the converges of the minimization algorithms in MINUIT. To alleviate this situation, a bunch of random numbers is chosen at the beginning of the fit, and as MINUIT varies E and B, the same set of random numbers are used. Configuration is chosen at the beginning of the fit once and for all.

5. CHAOTICITY AND CONDUCTIVITY MECHANISMS IN PMMA

Electrical charge transportation in nonconducting polymers is characterized by Schottky and Pool-Frenkel type conductivities[18]. The equation of transportation is given by the model;

$$j = j_0 e^{(\beta E)^{\frac{1}{2}}} \tag{5.1}$$

where j denotes the current density and j_0 is the saturation density of the nonconducting material. E is the strength of the electric field intensity and β is a proportionality constant. In the Schottky model β is given by

$$\beta = \beta_{sch} = \frac{e}{kT}\left[\frac{e}{4\pi\varepsilon\varepsilon'}\right]^{\frac{1}{2}} \tag{5.2}$$

In the Pool-Frenkel model β is given by

$$\beta = \beta_{pf} = 2\beta_{sch} = \frac{e}{kT}\left[\frac{e}{\pi\varepsilon\varepsilon'}\right]^{\frac{1}{2}} \tag{5.3}$$

where ε is the dielectric constant of the material and ε' is the dielectric constant of vacuum. T denotes temperature, k is the Boltzman constant and e is the electronic charge. Temperature plays a dominant role in the conductivity mechanisms of polymers, especially around the glass transition temperature which is 360K. Below 320K the conductivity can be modelled by the Schottky mechanism. Over 360K the Pool-Frenkel conductivity mechanism explains the situation. But between these temperatures conductivity mechanism of the polymers can not be completely explained by any of the two models.

Polymeric dielectric materials have very low conductivity. The micro- and macrostructure of polymeric dielectrics are sensitive to their thermal, mechanical and elec-

trical history. Polymers contain many impurities, additives and imperfections. These affect the reproducibility of conductivity measurements.

When an electric field is applied to a dielectric, bound and free charges interact with the electric field . This interaction causes the transient current observed in measurements. Transient current has a characteristic behavior, first it falls off which is called the polarization current and then it becomes steady. Some of the main causes of this behavior can be summarized as[6],

- Charging of the geometrical vacuum capacitance;
- Fast kinds of polarization, e.g. resonance and some types of dipole orientation.
- Slow types of dipole relaxation polarization.
- Flow of conduction current caused by the motion of charges injected from the electrodes or generated by thermal ionization of impurities or of the dielectric itself, or produced by photo-ionization or high-energy radiation ionization.
- Relaxation polarization of the Maxwell-Wagner type caused by micro- or macro-heterogeneities of a continuous or discrete nature.
- Electrode polarization due to complete or partial electrode blocking.
- Trapping of charge carriers in the bulk of the dielectric.

It is known that the polarization current depends on dipolar orientation in the direction of the applied field, free charge accumulation at structural or electrical inhomogeneities and space charge near the electrodes[26]. In many cases the absorption current responds over a wide interval of time according to the von Schweidler law,

$$i \propto t^{-k} \tag{5.4}$$

where $0 < k < 1$. But, it is known that the carrier transport in amorphous dielectrics have a non-Gaussian (or dispersive) character [5]. The field–time dependence of the the polarization current is given by [29],

$$i = A(T)\,[E(t)]^n\,t^{-k} \tag{5.5}$$

where $A(T)$ is a temperature-dependent factor. The exponent k is generally less than unity, but approaches this value as the trapping becomes increasingly effective, whereas n is expected to exceed unity [29]. However,under some conditions n can be less than unity for PMMA [5].

The current i which flows in organic polymers and amorphous materials on application of an external electric field E is known to depend on dipolar orientation in the direction of the field, resulting in free charge accumulation at structural or electrical inhomogeneities [26]. Frequently, the current follows the von Schweidler law over a wide interval of time according to

$$i(t) \propto t^{-k} \qquad \text{where} \qquad 0 < k < 1. \tag{5.6}$$

The experimental manifestations of dispersive (non-Gaussian) transient transport in disordered solids have been discussed by many authors [26, 27] and compared to the theoretical models. The general behavior of non-Gaussian transient transport of carriers in disordered solids is summarized in the following equations :

$$\begin{aligned} i(t) &\propto t^{-(1-\alpha)} \qquad \text{for} \qquad t < T_t, \\ i\,(t) &\propto t^{-(1-\beta)} \qquad \text{for} \qquad t > T_t, \end{aligned} \tag{5.7}$$

where T_t is interpreted as being the transit time of the carrier front whereas α and β are parameters describing the degree of dispersion. Such a power law in time of the form t^{-k} with k depending on a physical parameter is usually associated with multi fractal behavior. In particular, Yung Park [30] reports that relaxation resulting from the non-uniform but scaling fractal structures results in such a time behavior for the current.

We have observed that the transit time of charge carriers T_t as reflected by a change in the slope are related to the first zero crossing of the autocorrelation times observed during the time series analysis . This observation is in accordance with the

Onsager principle of regression fluctuations, which implies that C(t) approaches to zero as the fluctuations approaches an equilibrium value. The Figures 5.1 and 5.2 show the slope discontinuity at T_t and the behavior T_t as a function of applied potential. The table below compares the T_t values and the first zero crossing of the autocorrelation function suggesting that both occur at comparable times and the slope change reflects loss of correlation. The results are summarized in Table 5.1.

Table 5.1. Time when the slope is discontinuous compared to the first zero crossing of the autocorrelation function

E Field	T_q (Discontinuity)	First Zero of Auto-correlation
0.50 MV/m	1080	1186
1.00 MV/m	490	522
1.50 MV/m	440	509
2.00 MV/m	1150	1113
2.75 MV/m	560	549
3.25 MV/m	240	212

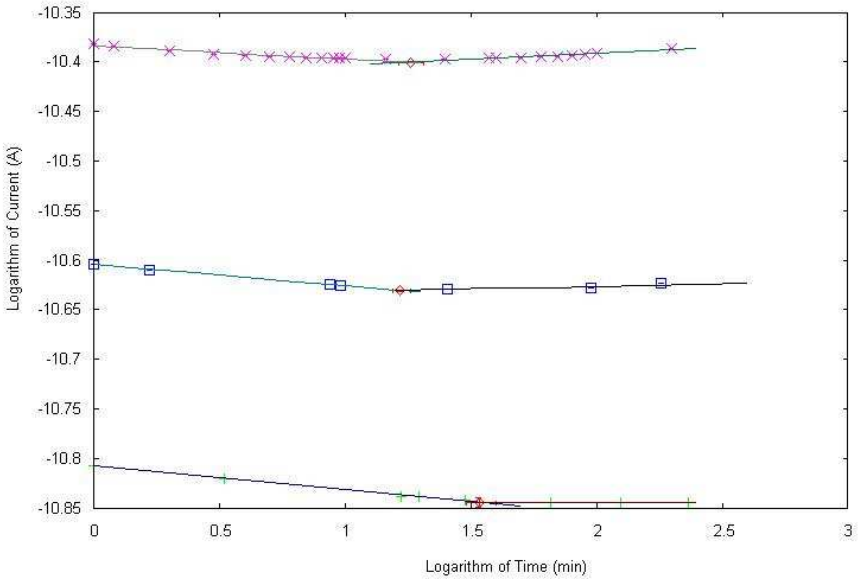

Figure 5.1. logarithmic scale plot of current versus time for 10V, 20V, 30V from bottom to top

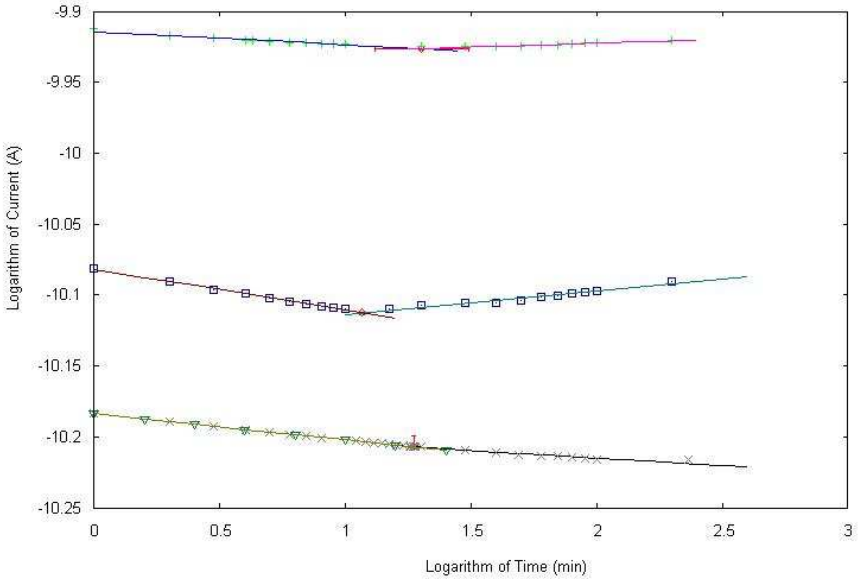

Figure 5.2. logarithmic scale plot of current versus time for 40V, 55V, 75V from bottom to top

5.1. Dependence Of The Transient Current on the Electric Field E

It is known that conductivity values are strongly field-dependent [33]. In [5] different regimes of electric field dependent conductivity has been identified. The field dependence is mostly attributed to trapping of free charge carriers in the volume of the dielectric during their motion due to the applied field whereas release from traps was considered to be thermally activated with a field-modified activation energy; [35] These charges are believed to be trapped in some of the localization states arising from the defects in the structure of the insulator such as impurities, dopants and dangling bonds. It has been suggested that side groups may act in a way similar to doped impurities [31]. Indeed, we have observed that the qualitative behavior of the transient current can be simulated by a transport process between randomly pinned impurity sites [12, 29]. The variation of Liapunov exponent with the applied electric field, given in Fig. 5.3 , suggests three different regimes. These regimes might be an outcome of competition between poloron and bipoloron states as well as the relaxation processes attributed to side chain motions [36].

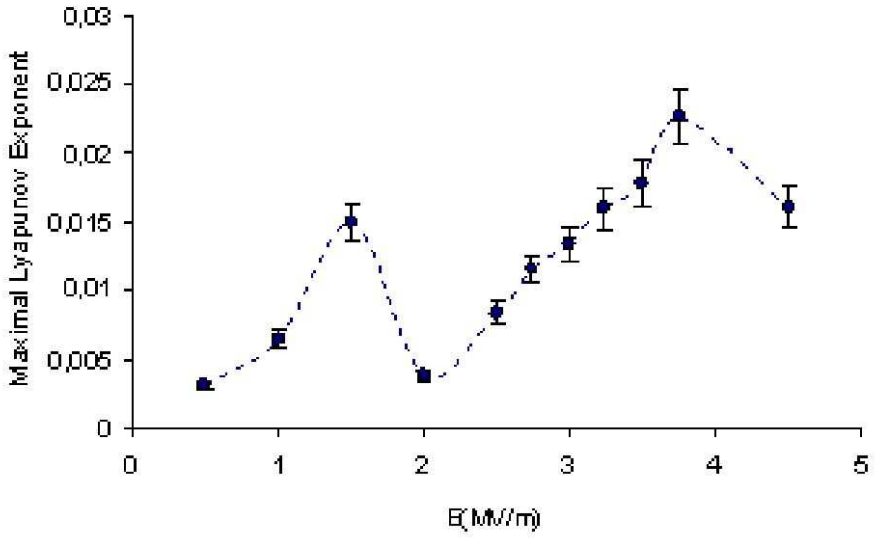

Figure 5.3. The voltage dependence of maximal Liapunov exponents

5.2. Temperature Dependence

The main relaxation processes in PMMA are α and β processes related to the cooperative dynamics (collective reorientation of the side groups with adjacent main chain segments —C—CH2—) and to the local dynamics (the reorientation of the polar ester side groups (—COOCH3) by local motions around the C—C bond [2]. Both processes (hence the glass transition temperature) are known to be dependent on the film thickness and the type of substrate [31]. Our sample is a 20 μm thick Al-PMMA-Al specimen. We have observed that the Liapunov exponents are temperature dependent and gives the characteristics of the α and β processes [5, 6, 35]. The two peaks observed in Fig. 5.4 correspond to the α and β peaks. The same type of behavior is observed for the information dimension as expected (since the Kaplan-Yorke conjecture relates the Liapunov exponents to the information dimension.).

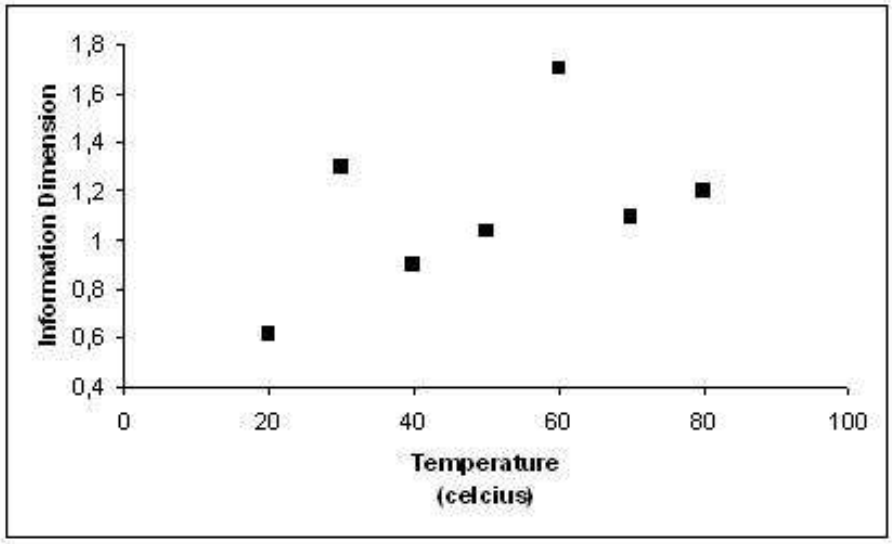

Figure 5.4. The temperature versus information dimension for the transient currents

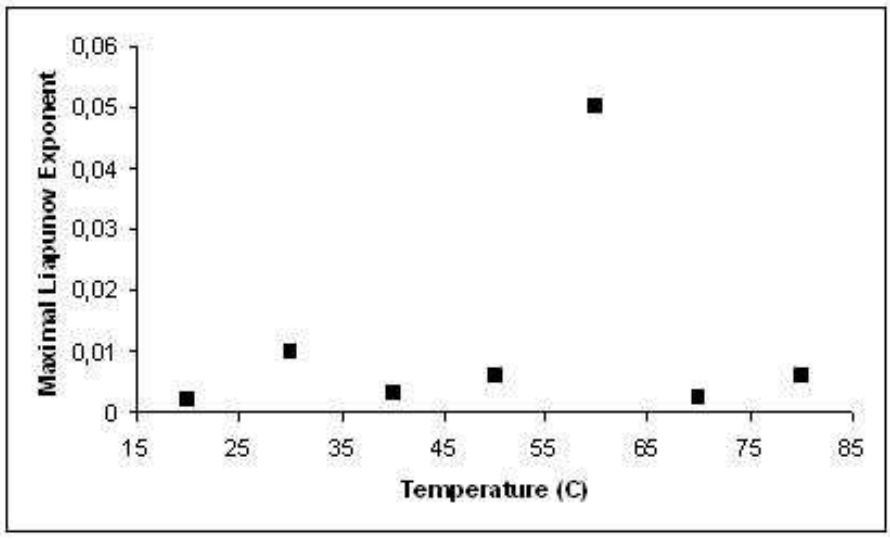

Figure 5.5. Temperature dependence of maximal Liapunov exponent

6. CONCLUSION

This work concentrated on experimentally studying the transient current and determining the maximal Liapunov exponent in the transient current in an AL-PMMA-AL specimen to ascertain chaotic behavior. A positive maximal Liapunov exponent in the range 0.01 to 0.05 has been observed for the temperature range of 293K-363K and for potential differences in the range 10-80 V. A reliable determination of the full Liapunov spectrum requires much larger data streams and processing. Both the false neighbor estimate and stabilization of the maximal exponent were used as different approaches in order to arrive at a satisfactory estimate of 4 as an embedding dimension. The complex structure of polymers (including impurities) implies many degrees of freedom and a multi-fractal structure. The computed information dimension traces the same behavior as the maximal Liapunov exponents as a function of temperature. This supports the observed multi-fractal power law behavior, t^{-k}.

We have observed that the transit time of charge carriers T_t as reflected by a change in the slope are related to the first zero crossing of the autocorrelation times observed during the time series analysis. In Ref.[5],it has been suggested that change in the current after $t > T_t$ might be due to physical aging processes of PMMA. The relation of aging processes to the two-time auto correlation function has been widely investigated in the literature [37, 38], but the exact relation between the autocorrelation function vs delay time requires a significantly larger volume of data.

The α process defines the glass transition temperature. It is also observed that the temperature dependence of the Liapunov exponents reflects the relaxation mechanisms, where one can identify the α and β processes by tracing the maximal Liapunov exponents as a function of temperature by looking at its peaks. The temperature corresponding to the second peak agrees with the glass transition temperature of the $20\mu m$ Al-PMMA-Al thin film and the first peak is in accordance with the β relaxation.

The first zero of the autocorrelation function and the first minimum of the mutual information function give widely different time scales one of which might be related to the fast relaxation processes (β relaxation) and the other to the slow relaxation process (α relaxation). The conduction mechanism or mechanisms in PMMA would thus involve two different time scales and steady state would only set in after both mechanisms have operated. The applied electric field can force the system by creating new traps and at same time acting as a dissipative agent by annihilating them. Such competing factors may have two significanses. They can either cause a bifurcation effect to an attractor or they can induce two characteristic and different time scales. When this is coupled with the complex structure of the polymer, it probably causes the chaotic time evolution of the current. This is a picture of quenched disorder [7] and helps us understand the embedding dimension estimate of 4 and observed multi-fractal behavior.

The experimental data can be fitted to a stretched exponential form qualitatively. This qualitative agreement and the quenched randomness in the experimental data suggest the charge density wave model. We manage to fit the CDW model to the experimental data qualitatively. The transient current through PMMA has two or possibly three regimes and this affects the quality of the fit.

APPENDIX A: THE CODE FOR STRETCHED EXPONENTIAL FIT

```
      IMPLICIT DOUBLE PRECISION (A-H,O-Z)
      DIMENSION X(20),G(20)
      PARAMETER (NTMAX=5000)
      EXTERNAL FCN,FUTIL

      OPEN (UNIT=5,FILE='MINUIT.DAT',STATUS='OLD')
      OPEN (UNIT=6,FILE='INPUTFILE.txt',STATUS='UNKNOWN')
      OPEN (UNIT=4,FILE='OUTPUTFILE',STATUS='UNKNOWN')
      CALL MINTIO(5 ,6,7)


C

C     Request FCN to read in (or generate random) data (IFLAG=1)

C      CALL FCN(NPAR,G,F,X,1, FUTIL)
C      CALL MINUIT(FCN,FUTIL)
       CALL MINNEW
C

      CALL FCN(NPAR,G,F,X,3,FUTIL)
      STOP

      END

C + DECKFCNK0
```

```
      SUBROUTINE FCN(NPAR,GIN,CHISQ,X,IFLAG,FUTIL)

C ************ DOUBLE PRECISION VERSION *************

      IMPLICIT DOUBLE PRECISION (A-H,O-Z)
      PARAMETER(NTMAX=5000)
      DIMENSION X(*),GIN(*),CUR(NTMAX),T(NTMAX),YFIT(NTMAX)
      EXTERNAL FUTIL
      IF(IFLAG.EQ.1) THEN
      DO 5 I=1,NTMAX
      READ(4,10,END=11) CUR(I)
      IF(CUR(I).LE.0.0) GOTO 11
10    FORMAT(F25.0)
5     CONTINUE
11    NTIME=I-1
      DO 12 I=1,NTIME
12    T(I)=I
      ENDIF
      CHISQ = 0.
      DT=1.0D-2
      DO 400 I= 1, NTIME

      TI = T(I)
c      CALL Fitdta(X,YFIT,NTIME,DT,iflag)

      YFIT(I) = X(1)*TI**-X(2)*EXP(-X(3)*TI**X(4))

      CHISQ = CHISQ + (CUR(I)-YFIT(I))**2/(CUR(I)*0.05)**2

      IF(IFLAG.EQ.3) WRITE(6,20) T(I),CUR(I),YFIT(I)
20    FORMAT(2X,F9.0,1X,2E12.3)
```

```
400   CONTINUE
      RETURN

      END

      LOGICAL FUNCTION INTRAC(DUMMY)
      DOUBLE PRECISION DUMMY
      INTRAC=.FALSE.
      RETURN
      END

      subroutine futil
      return
      end

C       THE SAME CODE MODIFIED TO FIND THE EXPONENTIAL FIT
C        USE DFLIB
      IMPLICIT DOUBLE PRECISION (A-H,O-Z)
      DIMENSION x(20),g(20)
      PARAMETER (ntmax=3000)
      EXTERNAL FCN,FUTIL

      OPEN (UNIT=5,FILE='MINUIT.DAT',STATUS='OLD')
      OPEN (UNIT=6,FILE='INPUTFILE.txt',STATUS='UNKNOWN')
      OPEN (UNIT=7,FILE='hede.OUT',STATUS='UNKNOWN')
      OPEN (UNIT=4,FILE='OUTPUTFILE.dat',STATUS='old')
      CALL MINTIO(5 ,6,7)

C
C     Request FCN to read in (or generate random) data (IFLAG=1)

C      CALL FCN(NPAR,G,F,X,1, FUTIL)
```

```
       CALL MINUIT(FCN,FUTIL)
C      CALL MINNEW
C

      CALL FCN(npar,g,f,x,3,FUTIL)
      STOP

      END

C + DECKFCNK0

      SUBROUTINE FCN(npar,gin,chisq,x,iflag,FUTIL)

C ************ DOUBLE PRECISION VERSION *************

      IMPLICIT DOUBLE PRECISION (A-H,O-Z)
      PARAMETER(NTMAX=3000)
      DIMENSION x(*),gin(*),cur(ntmax),YFIT(ntmax)
      EXTERNAL FUTIL
      IF(iflag.EQ.1) THEN
      DO 5 I=1,ntmax
c      READ(4,10,end=11) kint,cur(I)
    READ(4,10,end=11)cur(I)
    write(6,*)cur(I)
      IF(cur(I).LE.0.0) GOTO 11
c10    FORMAT(I3,1x,E18.0)
10    FORMAT(E18.0)
5     CONTINUE
11    NTIME=I-1

      ENDIF
      CHISQ = 0.
```

```
      DT=0.1
      CALL Fitdta(X,YFIT,NTIME,DT,iflag)
      DO 400 I= 1, NTIME




      YFIT(I) = X(1)*TI**-X(2)

      CHISQ = CHISQ + (CUR(I)-YFIT(I))**2/(CUR(I)*0.05)**2

      IF(IFLAG.EQ.3)  WRITE(6,20) CUR(I),YFIT(I)
20    FORMAT(2E12.3,2E12.3)
400   CONTINUE
      RETURN

      END

      LOGICAL FUNCTION INTRAC(DUMMY)
      DOUBLE PRECISION DUMMY
      INTRAC=.FALSE.
      RETURN
      END

      subroutine futil
      return
      end
```

APPENDIX B: THE FITTING CODE FOR THE CDW SIMULATION

```
C        USE DFLIB
       IMPLICIT DOUBLE PRECISION (A-H,O-Z)
       DIMENSION x(20),g(20)
       PARAMETER (ntmax=3000)
       EXTERNAL FCN,FUTIL
       common/statps/ nstat,npos,ntime
     common /rndms/norder,irnd,yarr(20100)
       write(*,*) ' enter no of passes'
       read(*,*) nstat
       write(*,*) ' enter no of impurity sites'
       read(*,*) npos
       write(*,*)  ' enter no of time steps <= ',NTMAX
       read(*,*) ntime
       norder=0
     irnd=0
       OPEN (UNIT=5,FILE='MINUIT.DAT',STATUS='OLD')
       OPEN (UNIT=6,FILE='OUTFILE.OUT',STATUS='UNKNOWN')
       OPEN (UNIT=7,FILE='hede.OUT',STATUS='UNKNOWN')
       OPEN (UNIT=4,FILE='INPUTFILE.dat',STATUS='UNKNOWN')
       CALL MINTIO(5 ,6,7)


C


C     Request FCN to read in (or generate random) data (IFLAG=1)
```

```
C       CALL FCN(NPAR,G,F,X,1, FUTIL)
        CALL MINUIT(FCN,FUTIL)
C       CALL MINNEW
C


      CALL FCN(npar,g,f,x,3,FUTIL)
      STOP

      END

C + DECKFCNK0

      SUBROUTINE FCN(npar,gin,chisq,x,iflag,FUTIL)

C ************ DOUBLE PRECISION VERSION *************

      IMPLICIT DOUBLE PRECISION (A-H,O-Z)
      PARAMETER(NTMAX=3000)
      DIMENSION x(*),gin(*),cur(ntmax),YFIT(ntmax)
      EXTERNAL FUTIL
      IF(iflag.EQ.1) THEN
      DO 5 I=1,ntmax
      READ(4,10,end=11) cur(I)
      IF(cur(I).LE.0.0) GOTO 11
10    FORMAT(E11.4)
5     CONTINUE
11    NTIME=I-1

      ENDIF
      CHISQ = 0.
      DT=1.0D-1
    WRITE(*,*)'CALLING FITDATA'
```

```
    CALL Fitdta(X,YFIT,NTIME,DT,iflag)
      DO 400 I= 1, NTIME




C      YFIT(I) = X(1)*EXP(-X(2)*TI**X(3))

      CHISQ = CHISQ + (CUR(I)-YFIT(I))**2/(CUR(I)*0.05)**2

      IF(IFLAG.EQ.3)  WRITE(6,20) CUR(I),YFIT(I)
20    FORMAT(2E12.3,2E12.3)
400   CONTINUE
      RETURN

      END

      LOGICAL FUNCTION INTRAC(DUMMY)
      DOUBLE PRECISION DUMMY
      INTRAC=.FALSE.
      RETURN
      END

      subroutine futil
      return
      end
c   THE SUBROUTINE WHICH SIMULATES THE CDW MODEL

      function rn(i)
          use Ziggurat

    implicit real*8(a-h,o-z)
```

```
c   T his assures that each MINUIT variation gets the same random numbers
    common /rndms/norder,irnd,yarr(20100)
    if(irnd. eq.0) then
      do i=1,20100
      yarr(i)=uni()
      enddo
    irnd=1
    endif
    if(norder.eq.0) norder=1
        rn=yarr(norder)
    norder=norder+1
      return
    end

      Subroutine Fitdta(x,curr,NTIME,DT,iflag)
C     This Sub Routine calculates simulated time development
c      use Ziggurat
      implicit real*8(a-h,o-z)
      implicit integer*4(i-n)
      COMMON/STATPS/ nstat, npos, ntime1
    common /rndms/norder,irnd,yarr(20100)
      parameter(NPOSM=10008,NTIMEM=3008,NSTATM=1)
      dimension Y(NPOSM,NTIMEM),current(NTIMEM),H(NPOSM),YPRIME(NPOSM,NT
    1IMEM)


      dimension X(*),CURR(*)
    WRITE(*,*)ntime,npos,ntimemax
      TWOPI=8.0D0*ATAN(1.0d0)
    B=X(1)
    E=X(2)
      DT=1.0d-1
```

```
c      open(unit=10, file='simcur.dat', status='unknown')

c     set the initial conditions
    norder=0
           do i=1,npos
             y(i,1)=rn(1)
           enddo

           do i=1,npos
        H(I)=rn(1)
           enddo

c         calculate YPRIME(NPOS,1)

                  DO J=2,NTIME+6
                      DO I=1,NPOS
c        each impurity site is assumed to be randomly away

        Y(I,J+1)=(1.0D0-2.0d0*B*DT)*Y(I,J) +DT*B*(Y(I-1,J)+Y(I+1,J))+
     1E*DT-DT*DSIN(TWOPI*(H(I)+Y(I,J)))
                       ENDDO
                       ENDDO

                   DO J=1,NTIME+7
                      DO I=1,NPOS
c        each impurity site is assumed to be randomly away
       YPRIME(I,J)=B*(Y(I+1,J)+Y(I-1,J)-2*Y(I,J))-SIN(TWOPI*(H(I)+Y(I,
    1J)))+E

                       ENDDO
                       ENDDO
```

```
c              write(,*)"current (j)=a/npos"
               DO J=1,NTIME+7
                  A=0
               DO I=1,NPOS
                    A=A+YPRIME(I,J)
                enddo
               current(J)=A/NPOS
c              write(*,*) current(J)
               enddo

               DO I=1,NTIME
                 CURR(I)=X(3)*current(i+7)/current(8)
      ENDDO
    WRITE(*,*)'GETTING OUT OF FITDATA'
    RETURN
      end
```

REFERENCES

1. Schuster, G. H., "Deterministic Chaos", *VCH*, Weinheim, Germany, 1988.

2. Lorenz, E. N., "Computational Chaos - A prelude to computational instability", *Physica D*, Vol.35, pp. 299-317, 1989.

3. Stewart, I., "Does God play with dice", *The Mathematics of Chaos*, New York: Gordon and Breach, pp. 141, 1970.

4. Hacinliyan, A., Y. Skarlatos, G.Sahin and G. Akin, " Signals of chaotic behavior in PMMA", *Chaos, Solitons and Fractals*, Vol.17, pp.575-585, 2003.

5. Mazur, K., "More data about dielectric and electret properties of poly(methyl methacrylate)", *Journal of Physics D*,Vol. 30, pp. 1383-1398, 1997.

6. Adamec, V. and J. H. Calderwood, "Electrical conduction and polarisation phenomena in polymers at low fields", *Journal of Physics D*, Vol. 11, pp. 781-800, 1978.

7. Erzan, A., E. Veermans, R. Heijung and L. Pietronero, " Glassy dynamics of pinned charge density waves.", *Phys. Rev. B*, Vol. 41, pp. 11522-11528, 1990.

8. Taken, F., "Detecting strange attractors in turbulence", *Lecture Notes in Mathematics*, Vol. 898, pp. 366-381, 1981.

9. Sauer, T., J. Yorke and M. Casdagli, "Embedology", *Journal of Statistical Physics*, Vol. 65, pp. 579-616, 1991.

10. Orear, J., *Notes on Statistics For Physicists: Revised*, http://nedwww.ipac.caltech.edu/level5/Sept01/Orear/Orear.html, 2001.

11. Abarbanel, H.D.I., *Analysis of Observed Chaotic Data.* , Springer Verlag, New

York, 1996.

12. Paladin, G. and A. Vulpani, "Anamolous scaling laws in multifractal objects", *Physics Reports*, Vol. 156, pp. 147-225, 1987.

13. Renyi, A., "Probability Theory", *North-Holland*, Amsterdam, 1970.

14. Hegger, R., H. Kantz and T. Schreiber, "Practical implementation of nonlinear time series methods: The TISEAN package", *CHAOS*, Vol.94, pp. 413-435, 1999.

15. Sano, M. and Y. Sawada, "Measurement of the Liapunov spectrum from a chaotic time series", *Physical Review Letters*, Vol. 55, pp. 1082-1085, 1985.

16. Kantz, H., "A rebust method to estimate the maximal Liapunov exponent of a time series", *Physics Letters A*, Vol. 185, pp. 77-87, 1994.

17. Abarbanel, H.D.I., R. Brown, J. J. Sidorowich and L.S. Tsimring, "The analysis of observed chaotic data", *Reviews of Modern Physics*, Vol. 65, pp. 1331-1392, 1993.

18. Efimenko, K., V. Rybka, V. Svorcik and W. Hnatowicz, "Mechanism of conductivity in metalpolymermetal structures", *Journal of Applied Physics A*, Vol. 68, pp. 479-482, 1999.

19. Kantz, H. and T. Schreiber, "Nonlinear Time Series Analysis" , *Cambridge University Press*, UK, 1997.

20. Pietronero, L., S. Strssler, S. Toombs, "Theory of the conductivity of the pinned Fröhlich charge density wave", *Phys. Rev. B*, Vol.12, pp. 5213-5220, 1975.

21. Erzan, A., E. Veermans, R. Hijungs and L. Pietronero, "Glassy Dynamics of Pinned Charge Density Waves: Numerical Simulations", *Physica A*, Vol.166, pp. 447-472, 1990.

22. Ediger, M.D., C. A. Angell and S.R. Nagel, "Supercooled liquids and glasses",

Journal of Chemistry, Vol. 100, pp. 13200-13212, 1996.

23. Fischer, K. H. and J. A. Hertz, "Spin Glasses", *Cambridge*, London, UK, 1991.

24. Wolfram, S., "The Mathematica Book", *Wolfram Media*, United States, 2003.

25. MINUIT, "Function Minimization and Error Analysis: Reference Manual 94.1", *CERN*, Geneva, Switzerland, 1994.

26. Das-Gupta, D. K., "Proc. 4th Int. Conf. on Conduction and Breakdown in Solid Dielectrics", *Sestri Levante (Piscataway, NJ: IEEE)*, 1992.

27. Scher, H. and E. W. Montroll, " Anamolous transit-time disperion in solids ", *Physical Review B*, Vol. 12, pp. 2455-2477, 1975.

28. Pfister, G. and C. Griffiths, "Temperature Dependence of Transient Hole Hopping Transport in Disordered Organic Solids ", *Phys. Rev. Lett.*, Vol. 40, pp. 659-662, 1978.

29. Sessler, G. M., " Electrets", *Springer*, Springer, 1980.

30. Park, Y., "Effect of Random Fractals on The Dielectric Relaxation of a Heterogeneous Medium", *Fractals*, Vol. 9, pp. 271-293, 2001.

31. Lewis, T. J., " Charge transport, charge injection and breakdown in polymeric insulators", *Journal of Physics D: Applied Physics*, Vol. 23, pp. 1469-1478, 1990.

32. Heuer, A. and P. Neu, " Tunneling dynamics of side chains and defects in proteins, polymer glasses, and OH-doped network glasses", *Journal of Chemical Physics*, Vol. 107, pp. 8686-8696, 1997.

33. Bellon, L., S. Ciliberto and C. Laroche, "Memory in the aging of a polymer glass", *Europhysics Letters*, Vol. 51, pp. 551-556, 2000.

34. Boettcher, S. and M. Paczuski, "Aging in a Model of Self-Organized Criticality", *Physical Review Letters*, Vol. 79, pp. 889-892, 1997.

35. Wubbenhorst, M., C.A. Murray and J. R. Dutcher, "Dielectric relaxations in ultrathin isotactic PMMA films and PS-PMMA-PS trilayer films", *European Physics Journal E*, Vol. 12, pp. 109-112, 2003.

36. Crissman, J. M., J. A. Sauer and A. E. Woodward, " Dynamic mechanical behavior of some high polymers at teperatures from 6K ", *Journal of Polymer Science A*, Vol. 2, pp. 5075-5091, 1964.

37. Viot, P., J. Talbot and G. Tarjus, "Slow Dynamics, aging and History-Dependent Effects in the Parking-Lot Model", *Fractals*, Vol. 11, pp. 185-196, 2003.

38. Ozeki, Y., "The aging relation for Ising spin glasses", *Journal of Physics: Condensed Matter*, Vol. 9, pp. 11171-11177, 1997.